Geoscience Frontiers 5 (2014) 261–276

Contents lists available at SciVerse ScienceDirect

China University of Geosciences (Beijing)

Geoscience Frontiers

journal homepage: www.elsevier.com/locate/gsf

Research paper

# Alkali feldspar syenites with shoshonitic affinities from Chhotaudepur area: Implication for mantle metasomatism in the Deccan large igneous province

K.R. Hari [a,*], N.V. Chalapathi Rao [b], Vikas Swarnkar [c], Guiting Hou [d]

[a] School of Studies in Geology and Water Resource Management, Pt. Ravishankar Shukla University, Raipur, Chhattisgarh, India
[b] Centre of Advance Study in Geology, Banaras Hindu University, Varanasi 221005, U.P., India
[c] Department of Civil Engineering, Yugantar Institute of Technology and Management, Rajnandgaon 491441, Chhattisgarh, India
[d] The Key Laboratory of Orogenic Belts and Crustal Evolution, Ministry of Education, School of Earth and Space Sciences, Peking University, Beijing 100871, China

ARTICLE INFO

*Article history:*
Received 5 February 2013
Received in revised form
25 June 2013
Accepted 30 June 2013
Available online 20 July 2013

*Keywords:*
Alkali feldspar syenite
Deccan large igneous province
Mineralogy
Geochemistry
Shoshonite
Mantle metasomatism

ABSTRACT

Two petrologically distinct alkali feldspar syenite bodies (AFS-1 and AFS-2) from Chhotaudepur area, Deccan Large Igneous Province are reported in the present work. AFS-1 is characterized by hypidiomorphic texture and consists of feldspar ($Or_{55}Ab_{43}$ to $Or_{25}Ab_{71}$), ferro-pargasite/ferro-pargasite hornblende, hastingsite, pyroxene ($Wo_{47}$, $En_5$, $Fs_{46}$), magnetite and biotite. AFS-2 exhibits panidiomorphic texture with euhedral pyroxene ($Wo_{47\text{-}50}$, $En_{22\text{-}39}$, $Fs_{12-31}$) set in a groundmass matrix of alkali feldspar ($Or_{99}Ab_{0.77}$ to $Or_{1.33}Ab_{98}$), titanite and magnetite. In comparison to AFS-1, higher elemental concentrations of Ba, Sr and ∑REE are observed in AFS-2. The average peralkaline index of the alkali feldspar syenites is ~1 indicating their alkaline nature. Variation discrimination diagrams involving major and trace elements and their ratios demonstrate that these alkali feldspar syenites have a shoshonite affinity but emplaced in a within-plate and rifting environment. No evidence of crustal contamination is perceptible in the multi-element primitive mantle normalized diagram as well as in terms of trace elemental ratios. The enrichment of incompatible elements in the alkali feldspar syenites suggests the involvement of mantle metasomatism in their genesis.



## 1. Introduction

Deccan large igneous province with an eruptive aerial extent of $10^6$ km$^2$, is one of the largest igneous provinces of the world with a time span of 61–67 Ma (Hofmann et al., 2000; Widdowson et al., 2000; Chenet et al., 2007; Hooper et al., 2010). Tholeiitic basalts and its derivatives constitute the dominant rock types of the Deccan LIP with alkali basalts, carbonatites, lamprophyres, and syenites in minor proportions. A substantial increase of at least $8.5 \times 10^4$ km$^2$ areal extension of Deccan LIP has been recently recognized on the basis of the Deccan-age of the Chhattisgarh subsurface dykes and the Mainpur orangeites (Chalapathi Rao et al., 2011a). Lehmann et al. (2010), Chalapathi Rao and Lehmann (2011) and Chalapathi Rao et al. (2011b) have also recently identified kimberlite (orangeites) eruptions from Bastar craton of Central India that are synchronous with the main phase of the Deccan flood basalts at 65 Ma. The widespread presence of isolated exposures of alkali olivine basalt, rhyolites, lamprophyres, alkaline plugs and carbonatites located in different parts of western part of India, Saurasthra-Kutch region and also along the Narmada – Son rift valley render the petrogenesis of Deccan LIP intriguing. The alkali igneous complexes of nephelinite-carbonatite affinities are considered to be either early or late phases of magmatism with reference to the main pulse of the Deccan volcanic eruption episode (e.g. Basu et al., 1993; Simonetti et al., 1998). A number of mafic dykes are also associated with the Deccan LIP (Ray et al., 2007; Vanderkluysen et al., 2011). Ju et al. (2013) while modelling the palaeostress fields of the Deccan volcanic province, argued that the

* Corresponding author. Tel.: +91 98279 84622.
*E-mail addresses:* krharigeology@gmail.com, krhari2005@rediffmail.com (K.R. Hari).

Peer-review under responsibility of China University of Geosciences (Beijing)

Production and hosting by Elsevier

1674-9871/$ – see front matter © 2013, China University of Geosciences (Beijing) and Peking University. Production and hosting by Elsevier B.V. All rights reserved.
http://dx.doi.org/10.1016/j.gsf.2013.06.007

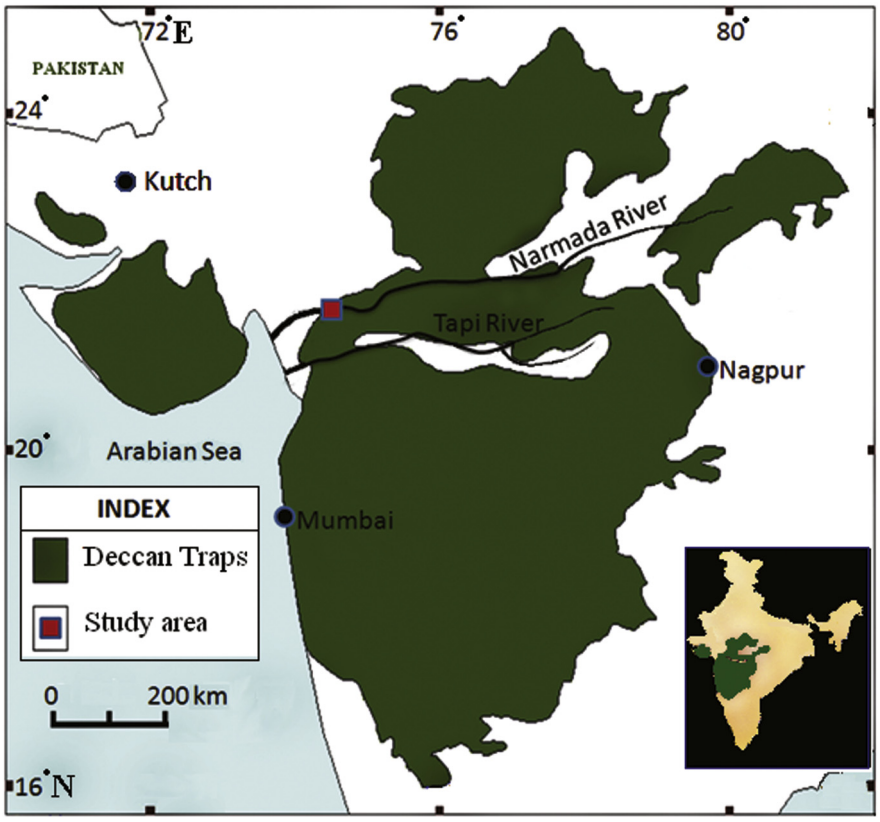


**Figure 1.** Map of Deccan Traps showing the location of study area.

dykes from Lower Narmada Valley were formed earlier followed by dykes from the Nasik-Pune region and western coastal part of India.

In the Deccan LIP, a few exposures of syenite have been reported from Murud-Janjira (Dessai and Bodas, 1984), Mundwara igneous complex (Chakraborty, 1979) as well as from the Chhotaudepur area (Sukheswala and Sethna, 1973; Gwalani et al., 1994). These syenite bodies are relatively least studied. In this communication, we present mineralogy and geochemistry of two syenite bodies near the Phenai Mata igneous complex (AFS-1) and Karajwant (AFS-2) of the Chhotaudepur sub-province of the Deccan LIP (Fig. 1) and infer their petrogenesis. The alkali feldspar syenite near Phenai Mata igneous complex (AFS-1) was reported by earlier workers as 'Pulaskite' (Sukheswala and Sethna, 1973; Gwalani et al., 1994)

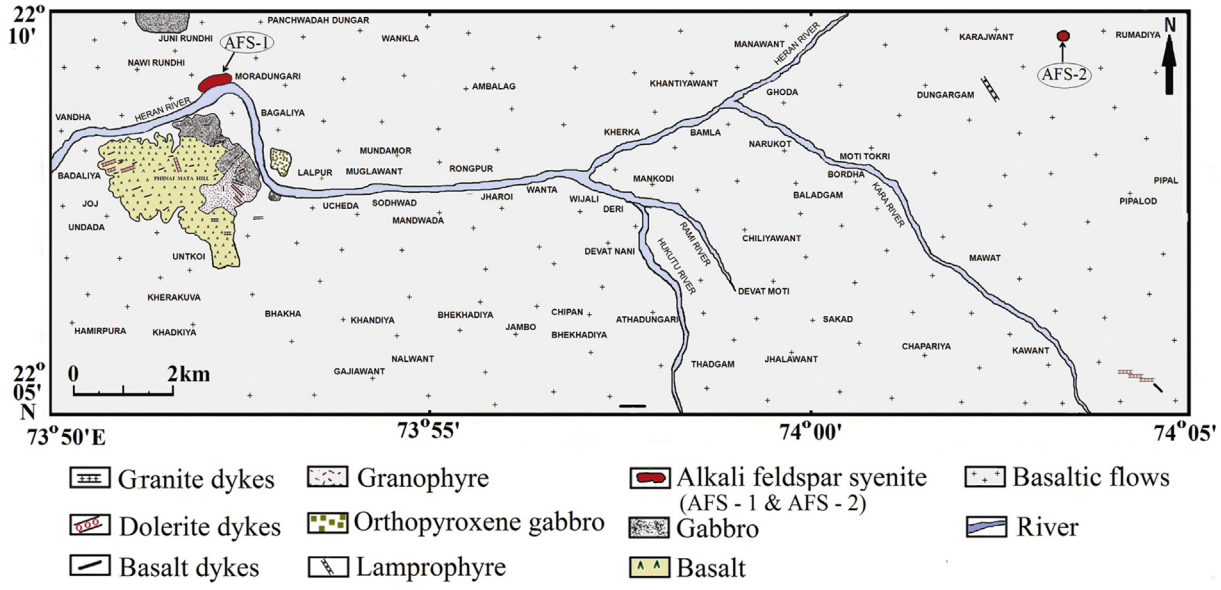


**Figure 2.** Geological map of the part of Chhotaudepur province exhibiting the exposures of alkali feldspar syenite (modified after Gwalani et al., 1994; Kumar, 1996).

**Figure 3.** Photograph showing the exposure of alkali feldspar syenite (AFS-2) near Karajwant.

**Table 1**
Mineral chemical analyses of feldspar from AFS-1.

| | 1 | 2 | 3 | 4 | 5 |
|---|---|---|---|---|---|
| $SiO_2$ | 65.32 | 66.02 | 65.71 | 65.95 | 67.41 |
| $TiO_2$ | 0.04 | 0.02 | 0.09 | 0.01 | 0.04 |
| $Al_2O_3$ | 18.45 | 18.45 | 18.41 | 18.32 | 19.18 |
| $Cr_2O_3$ | 0.00 | 0.00 | 0.05 | 0.00 | 0.00 |
| FeO | 0.15 | 0.11 | 0.11 | 0.17 | 0.09 |
| MnO | 0.00 | 0.00 | 0.00 | 0.05 | 0.00 |
| MgO | 0.00 | 0.00 | 0.01 | 0.00 | 0.00 |
| CaO | 0.33 | 0.24 | 0.17 | 0.23 | 0.67 |
| $Na_2O$ | 5.50 | 5.11 | 4.73 | 5.24 | 8.00 |
| $K_2O$ | 8.20 | 8.53 | 9.29 | 8.50 | 4.37 |
| ZnO | 0.19 | 0.00 | 0.00 | 0.00 | 0.00 |
| $P_2O_5$ | 0.00 | 0.00 | 0.00 | 0.00 | 0.00 |
| Total | 98.18 | 98.48 | 98.57 | 98.47 | 99.78 |
| Formula (on the basis of 32 oxygen) | | | | | |
| Si | 11.978 | 12.042 | 12.018 | 12.043 | 11.975 |
| Ti | 0.006 | 0.003 | 0.012 | 0.001 | 0.005 |
| Al | 4.009 | 3.987 | 3.989 | 3.964 | 4.037 |
| Cr | 0.000 | 0.000 | 0.007 | 0.000 | 0.000 |
| Fe | 0.023 | 0.017 | 0.017 | 0.026 | 0.013 |
| Mn | 0.000 | 0.000 | 0.000 | 0.008 | 0.000 |
| Mg | 0.000 | 0.000 | 0.003 | 0.000 | 0.000 |
| Ca | 0.065 | 0.047 | 0.033 | 0.045 | 0.128 |
| Na | 1.956 | 1.807 | 1.677 | 1.855 | 2.756 |
| K | 1.918 | 1.985 | 2.168 | 1.980 | 0.990 |
| Zn | 0.026 | 0.000 | 0.000 | 0.000 | 0.000 |
| P | 0.000 | 0.000 | 0.000 | 0.000 | 0.000 |
| Or | 48.69 | 51.71 | 55.91 | 51.03 | 25.56 |
| Ab | 49.66 | 47.07 | 43.24 | 47.81 | 71.14 |
| An | 1.65 | 1.22 | 0.85 | 1.16 | 3.30 |

whereas alkali feldspar syenite plug near Karajwant (AFS-2) is reported for the first time in this work. We suspect that the earlier reporting of 'Phonolite plug' near Karajwant by Gwalani et al. (1994) may be similar to AFS-2 alkali feldspar syenite as the geochemical data reported is similar to that generated in this study. Ray et al. (2003), on the basis of $^{40}Ar/^{39}Ar$, obtained an age of 65.2 ± 0.7 Ma for a Phonolite plug from near-by area.

## 2. Field relations

The Ambadungar alkaline igneous complex in the south-eastern corner and the Phenai Mata igneous complex in the western part are the two main igneous complexes in Chhotaudepur sub-province. The stratigraphic succession of this area includes Bagh Sandstone of Cretaceous age underlying the Deccan Trap basaltic flows (Gwalani et al., 1993, 1994). Ambadungar complex comprises calcite - carbonatite with small plugs of red-brown ankeritic-carbonatite (Sukeshwala and Avasia, 1972; Simonetti et al., 1998). Nepheline syenite dykes and plugs are reported from the low lying areas of Ambadungar dome (Viladkar, 1984; Gwalani et al., 1994). The Phenai Mata igneous complex comprises tholeiitic basalts, granophyres, gabbro, dyke-lets of granite with small dykes of dolerite (Kumar, 1996, 2003). Recently, Hari et al. (2011) reported orthopyroxene gabbro from this area. Basu et al. (1993) based on $^{40}Ar/^{39}Ar$ dating, measured an age of 65 Ma for the gabbro from this igneous complex. Chhotaudepur sub-province with dyke swarms of basalt, dolerite, lamprophyre, tinguaites, etc. are seen traversing through Deccan basalt (Sukeshwala and Avasia, 1972; Karkare and Srivastava, 1990; Viladkar and Avasia, 1992; Hari and Swarnkar, 2011).

A small exposure of about 0.40 $km^2$ aerial extent of alkali feldspar syenite (AFS-1) (Fig. 2) is located just north of Phenai Mata igneous complex (73°52′04.9″ E, 22°08′56.98″ N). Another exposure of alkali feldspar syenite (AFS-2) occurs as an isolated circular small hill (74°03′15.2″ E, 22°09′39.8″ N) of about 200 m high above MSL (Fig. 3) located near Karajwant. The present paper dwells on the mineralogy and geochemistry of these two syenite bodies.

## 3. Petrography

Petrographic studies reveal that quartz is entirely absent in the two syenites. K- feldspar is the predominant phase whereas plagioclase feldspar constitutes an accessory phase. Amphibole, pyroxene, titanite, opaques and few biotite flakes constitute rest of the minerals. Both the syenites can be categorized as alkali feldspar syenite as per the QAP discrimination diagram (after Streckeisen, 1974).

Electron microprobe analysis (by CAMECA SX100) of the minerals present in both AFS-1 and AFS-2 were carried out at the Mineral Resources, Clausthal University of Technology, Germany as

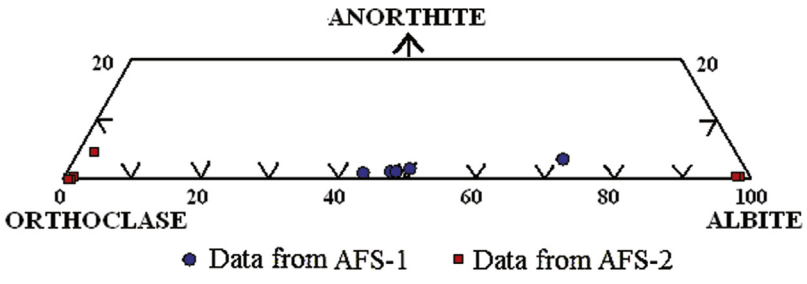


**Figure 4.** Mineral composition of feldspars in the Or-Ab-An diagram.

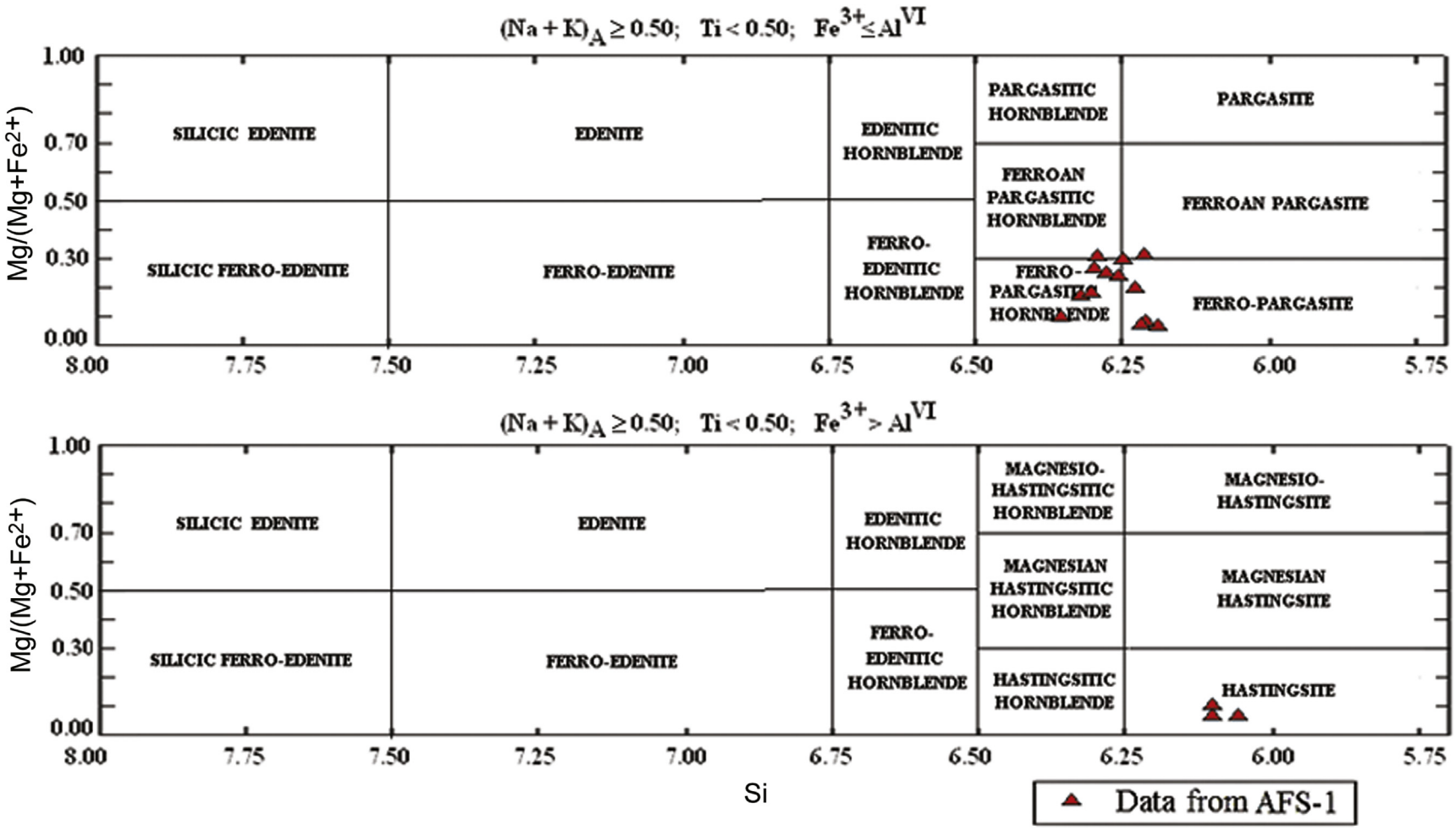


**Figure 5.** Figure showing the classification of amphibole on the basis of Si and Mg/(Mg + $Fe^{2+}$) (after Leake, 1978). Note that the amphibole in AFS-1 falls in hastingsite, ferro-pargasite hornblende and ferro-pargasite fields.

well as at the Wadia Institute of Himalayan Geology at Dehradun, India. A beam current of 20 nA, acceleration voltage of 15 kV and beam diameter of 1 μm was used. Both natural as well as synthetic standards were employed.

The syenite exposed near Phenai Mata (AFS-1) exhibits hypidiomorphic texture with alkali feldspar, amphibole, pyroxene, opaques and few grains of biotite. Feldspar is the dominant mineral and constitutes about 70% of this rock. Feldspar exhibits dusty appearance and in some cases, kaolinization is also noticeable. Perthitic texture is very common in the feldspars. The feldspar composition varies from $Or_{55}Ab_{43}$ to $Or_{25}Ab_{71}$ (Table 1, Fig. 4). Amphibole is the next dominant mineral in all thin sections. Two varieties of amphiboles are noticeable (i) ferro-pargasite/ferro-pargasitic hornblende and (ii) hastingsite (Fig. 5). Ferro-pargasite/Ferro-pargasitic hornblende exhibit distinct pleochroism from greenish yellow to light brown. Most of the grains have subhedral outline. Some of these grains exhibit simple twinning also. The mineral chemistry (Table 2) reveals that $TiO_2$ in these minerals varies from 2.58 to 3.13 wt.%. High MgO (2.91–5.66 wt.%) and low FeO (22.01–25.78 wt.%) are noticeable in these grains. Highly pleochroic hastingsite occur as coronal rims around ferro-pargasite (Fig. 6A) and also as discrete anhedral grains. Hastingsite grains show yellowish green, brownish green and bluish green pleochroic colours. The mineral chemistry reveals that hastingsite has lower MgO (0.87–1.66 wt.%), higher FeO (27.62–30.54 wt.%) and lower $TiO_2$ (0.45–1.97 wt. %) than ferro-pargasite and ferro-pargasitic hornblende. A few pyroxene grains observed in the sections are of ferro-hedenbergite (Table 3, Fig. 7). The opaques identified under the microscope are magnetite and their mineral chemistry is given in Table 4. A few biotite flakes are also perceptible in some sections.

The syenite from AFS-2 locality exhibits porphyritic texture with phenocrysts of pyroxene set in a matrix of feldspars, green coloured glass and opaques (Fig. 6B and C). Most of the pyroxene have euhedral outline exhibiting panidiomorphic texture. Pyroxene grains are green coloured and show faint pleochroism from pale green to yellowish green. Some grains exhibit zoning also. The mineral chemistry reveals enrichment of Mg towards the core of these mineral in many cases (Table 5). The pyroxene can be grouped under salite and ferrosalite (Fig. 7). The feldspar grains have subhedral outline and in most of the cases, slight alteration is noticeable. All the grains have a composition of $Or_{99}Ab_{0.77}$ to $Or_{1.33}Ab_{98}$ (Table 6, Fig. 4). Few euhedral colourless titanite grains are noticeable in the sections (Table 7) and the opaques are magnetite (Table 8).

## 4. Geochemistry

Twelve representative samples were analysed for their major elements by XRF and the trace elements by ICP-MS. The analyses were carried out at the National Geophysical Research Institute, Hyderabad, India (sample from AFS-1 location) and Wadia Institute of Himalayan Geology, India (samples from AFS-2 location), and the data are presented in Tables 9 and 10. Enrichment of $SiO_2$ is noticeable in all the samples of AFS-1. With the exception of one sample (GR-2D), all the other three samples of AFS-1 alkali feldspar syenite have low normative quartz contents. Slightly higher CaO contents are noticeable in all the samples of AFS-2 which may be due to the higher content of pyroxene in them. All the samples of AFS-2 are nepheline normative and in three samples, acmite is noticeable in the norm. High total alkali content (~10 wt.%) and REE concentrations are noticeable in both the syenites. However, Ba, Sr and ∑REE concentrations are higher in AFS-2 alkali feldspar syenite than AFS-1 alkali felspar syenite. The peralkaline index (molecular ratio [(Na + K)/Al]) of AFS-1 samples (0.73–0.96) is slightly lower compared to that of AFS-2 samples (0.87–1.06). The average peralkaline indices of the samples from AFS-1 (0.80) and AFS-2 (0.98) are close to 1.

**Table 2**
Mineral chemical analyses of amphibole from AFS-1.

| | Ferro-pargasite hornblede/ferro-pargasite | | | | | | | | | Hastingsite | | | | | | |
|---|---|---|---|---|---|---|---|---|---|---|---|---|---|---|---|---|
| | 1 | 2 | 3 | 4 | 5 | 6 | 7 | 8 | 9 | 10 | 11 | 12 | 13 | 14 | 15 | 16 |
| $SiO_2$ | 39.30 | 38.91 | 38.83 | 38.34 | 38.92 | 38.68 | 38.39 | 37.33 | 38.33 | 36.60 | 36.50 | 36.48 | 37.17 | 36.99 | 38.15 | 36.84 |
| $TiO_2$ | 3.05 | 2.85 | 2.89 | 2.69 | 3.13 | 2.79 | 2.58 | 2.75 | 2.61 | 1.64 | 0.45 | 0.87 | 1.97 | 1.74 | 1.63 | 1.71 |
| $Al_2O_3$ | 10.47 | 10.32 | 10.43 | 10.33 | 10.55 | 10.37 | 10.28 | 9.89 | 10.26 | 10.58 | 10.67 | 10.74 | 11.16 | 11.03 | 10.08 | 11.12 |
| $Cr_2O_3$ | 0.00 | 0.01 | 0.00 | 0.00 | 0.04 | 0.00 | 0.00 | 0.11 | 0.09 | 0.02 | 0.00 | 0.04 | 0.00 | 0.00 | 0.00 | 0.00 |
| FeO | 22.01 | 23.32 | 22.89 | 24.44 | 22.19 | 23.68 | 25.78 | 24.60 | 25.57 | 30.54 | 30.13 | 29.81 | 27.62 | 28.23 | 27.97 | 28.45 |
| MnO | 0.58 | 0.57 | 0.51 | 0.60 | 0.51 | 0.70 | 0.75 | 0.85 | 0.92 | 0.80 | 1.06 | 1.04 | 1.23 | 1.05 | 1.12 | 1.18 |
| MgO | 5.44 | 4.65 | 5.32 | 4.10 | 5.66 | 4.31 | 2.91 | 3.31 | 2.99 | 0.87 | 0.98 | 0.87 | 1.21 | 1.09 | 1.66 | 0.92 |
| CaO | 10.72 | 10.77 | 10.77 | 10.80 | 11.13 | 10.93 | 10.23 | 10.85 | 10.22 | 10.10 | 10.30 | 10.38 | 10.60 | 10.64 | 10.30 | 9.76 |
| $Na_2O$ | 2.44 | 2.36 | 2.40 | 2.42 | 2.49 | 2.46 | 2.53 | 2.59 | 2.29 | 2.54 | 2.48 | 2.39 | 2.34 | 2.34 | 2.55 | 2.39 |
| $K_2O$ | 1.70 | 1.68 | 1.73 | 1.65 | 1.73 | 1.63 | 1.64 | 1.73 | 1.73 | 1.80 | 1.79 | 1.85 | 1.73 | 1.68 | 1.69 | 1.68 |
| ZnO | 0.15 | 0.00 | 0.09 | 0.08 | 0.10 | 0.11 | 0.21 | 0.00 | 0.00 | 0.09 | 0.05 | 0.12 | 0.06 | 0 | 0.16 | 0.18 |
| $P_2O_5$ | 0.00 | 0.01 | 0.00 | 0.02 | 0.06 | 0.00 | 0.00 | 0.07 | 0.00 | 0.02 | 0.00 | 0.00 | 0.00 | 0.04 | 0.00 | 0.02 |
| Total | 95.88 | 95.46 | 95.86 | 95.46 | 96.49 | 95.68 | 95.3 | 94.07 | 95.01 | 95.62 | 94.41 | 94.59 | 95.08 | 94.82 | 95.32 | 94.25 |
| Formula (on the basis of 23 oxygen) | | | | | | | | | | | | | | | | |
| Si | 6.288 | 6.294 | 6.246 | 6.250 | 6.208 | 6.268 | 6.308 | 6.227 | 6.309 | 6.171 | 6.231 | 6.209 | 6.206 | 6.212 | 6.354 | 6.228 |
| Ti | 0.367 | 0.347 | 0.350 | 0.330 | 0.376 | 0.340 | 0.319 | 0.345 | 0.323 | 0.208 | 0.058 | 0.111 | 0.247 | 0.220 | 0.204 | 0.217 |
| Al | 1.985 | 1.978 | 1.988 | 1.995 | 1.994 | 1.991 | 2.001 | 1.955 | 2.001 | 2.114 | 2.158 | 2.166 | 2.208 | 2.195 | 1.989 | 2.227 |
| Cr | 0 | 0.001 | 0.000 | 0.000 | 0.005 | 0.000 | 0.000 | 0.015 | 0.012 | 0.003 | 0.000 | 0.005 | 0.000 | 0.000 | 0.000 | 0.000 |
| Fe | 2.945 | 3.155 | 3.079 | 3.332 | 2.960 | 3.209 | 3.542 | 3.432 | 3.520 | 4.306 | 4.302 | 4.244 | 3.857 | 3.965 | 3.896 | 4.022 |
| Mn | 0.079 | 0.078 | 0.070 | 0.083 | 0.069 | 0.096 | 0.104 | 0.120 | 0.128 | 0.114 | 0.153 | 0.150 | 0.174 | 0.149 | 0.158 | 0.169 |
| Mg | 1.297 | 1.121 | 1.275 | 0.996 | 1.346 | 1.041 | 0.713 | 0.823 | 0.734 | 0.219 | 0.249 | 0.221 | 0.301 | 0.273 | 0.412 | 0.232 |
| Ca | 1.838 | 1.867 | 1.856 | 1.887 | 1.902 | 1.898 | 1.801 | 1.939 | 1.803 | 1.825 | 1.884 | 1.893 | 1.896 | 1.915 | 1.838 | 1.768 |
| Na | 0.757 | 0.740 | 0.749 | 0.765 | 0.770 | 0.773 | 0.806 | 0.838 | 0.731 | 0.830 | 0.821 | 0.789 | 0.758 | 0.762 | 0.824 | 0.783 |
| K | 0.347 | 0.347 | 0.355 | 0.343 | 0.352 | 0.337 | 0.344 | 0.368 | 0.363 | 0.387 | 0.390 | 0.402 | 0.369 | 0.360 | 0.359 | 0.362 |
| Zn | 0.018 | 0.000 | 0.011 | 0.010 | 0.012 | 0.013 | 0.026 | 0.000 | 0.000 | 0.011 | 0.006 | 0.015 | 0.007 | 0.000 | 0.020 | 0.023 |
| P | 0.000 | 0.001 | 0.000 | 0.003 | 0.008 | 0.000 | 0.000 | 0.010 | 0.000 | 0.003 | 0.000 | 0.000 | 0.000 | 0.006 | 0.000 | 0.003 |
| Fe | **69.43** | **73.78** | **70.72** | **76.99** | **68.74** | **75.51** | **83.24** | **80.66** | **82.75** | **95.16** | **94.53** | **95.05** | **92.76** | **93.56** | **90.44** | **94.55** |
| Mg | **30.58** | **26.27** | **29.28** | **23.01** | **31.26** | **24.49** | **16.76** | **19.34** | **17.25** | **4.84** | **5.47** | **4.95** | **7.24** | **6.44** | **9.56** | **5.45** |

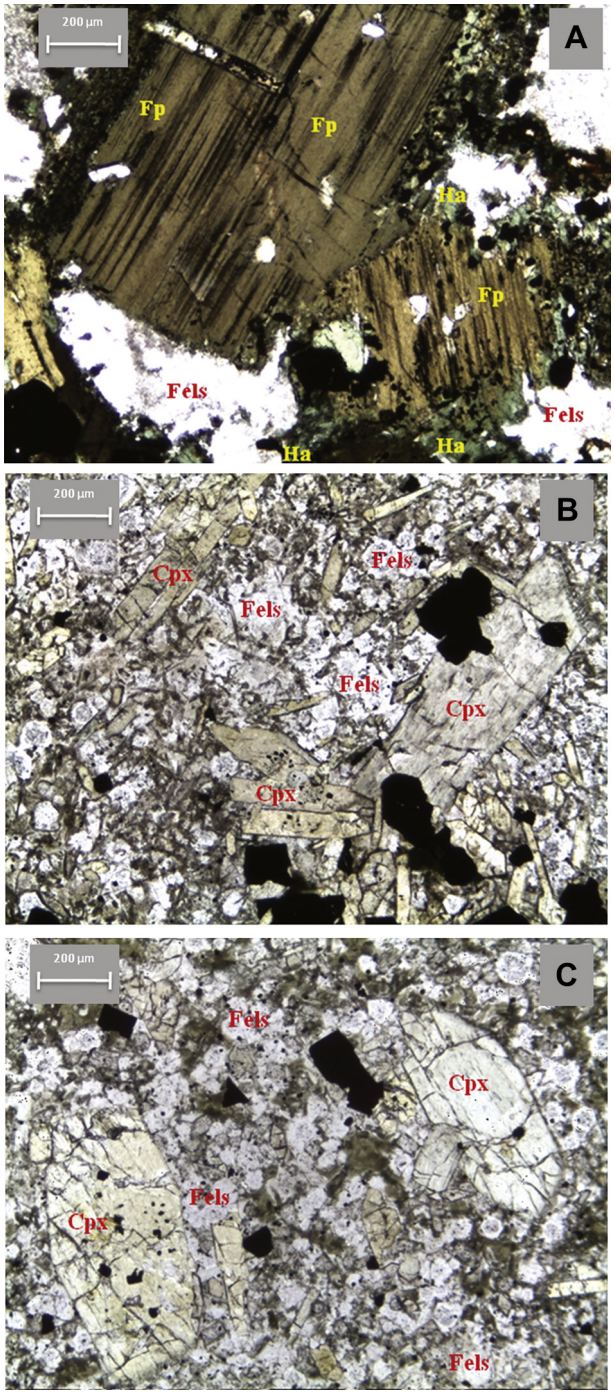


**Figure 6.** (A) Photomicrograph exhibiting hastingsite (bluish green coloured) seen as coronal rims around ferro-pargasite (light and dark brown coloured) in AFS-1 alkali feldspar syenite. Fp – ferro-pargasite, Ha – hastingsite, Fels – feldspar. (B and C) Photomicrographs showing euhedral clinopyroxene grains set in a metrix of feldspar, opaques and glass. Cpx–clinopyroxene, Fels– feldspar.

## 5. Petrogenesis

Both alkali feldspar syenites have high alkali (~10 wt.%), Rb, Ba and ∑REE contents exhibiting their alkaline nature. All the samples fall in the 'alkaline' field when plotted in the $SiO_2$ vs. total alkali diagram (field demarcation after Irvine and Baragar, 1971; not shown). Further, the peralkaline index of these samples is nearer to 1. The alkaline nature of these rocks is further substantiated by the steep REE chondrite-normalized pattern (Fig. 8) and high La/Yb ratios (57–63) of the samples.

**Table 3**
Mineral chemical analyses of pyroxene from AFS-1.

| | 1 | 2 |
|---|---|---|
| $SiO_2$ | 47.33 | 47.36 |
| $TiO_2$ | 0.19 | 0.19 |
| $Al_2O_3$ | 1.86 | 1.86 |
| $Cr_2O_3$ | 0.00 | 0.01 |
| FeO | 23.82 | 23.55 |
| MnO | 1.45 | 1.40 |
| MgO | 1.63 | 1.85 |
| CaO | 20.29 | 20.21 |
| $Na_2O$ | 0.99 | 1.02 |
| $K_2O$ | 0.03 | 0.01 |
| ZnO | 0.08 | 0.00 |
| $P_2O_5$ | 0.00 | 0.03 |
| Total | 97.66 | 97.51 |
| Formula (on the basis of 6 oxygen) | | |
| Si | 1.964 | 1.965 |
| Ti | 0.006 | 0.006 |
| Al | 0.092 | 0.092 |
| Cr | 0.000 | 0.000 |
| Fe | 0.827 | 0.817 |
| Mn | 0.051 | 0.049 |
| Mg | 0.101 | 0.114 |
| Ca | 0.902 | 0.899 |
| Na | 0.080 | 0.082 |
| K | 0.002 | 0.001 |
| Zn | 0.003 | 0.000 |
| P | 0.000 | 0.001 |
| Ca | 47.95 | 47.85 |
| Mg | 5.37 | 6.07 |
| Fe + Mn | 46.68 | 46.09 |

When the syenite and related rocks from Deccan volcanic provinces (Murud-Janjira, Mundwara as well as the present study) are plotted in the $SiO_2$ vs. $K_2O$ diagram (Fig. 9A), they all fall in the shoshonite field. When plotted in $K_2O$ vs. $Na_2O$ diagram (Fig. 9B), the samples from AFS-1, Murud-Janjira and Mundwara fall exclusively in shoshonitic field whereas few samples of AFS-2 fall in the shoshonitic field and rest in the calc-alkaline field but are very close to the demarcation line between shoshonitic field and calc-alkaline field. The shoshonitic rocks are geochemically characterized by high total alkalies ($K_2O + Na_2O > 5\%$), high $K_2O/Na_2O$ ratios (>0.6 if $SiO_2$ ~50 wt.%, >1.0 if $SiO_2$ ~55 wt.%), low $TiO_2$, high but variable $A1_2O_3$ (14–19 wt.%) and strong enrichment in LILE and LREE (Morrison, 1980). In the present case, all the samples exhibit high $K_2O + Na_2O$ (8.73–12.23 wt.%), $Al_2O_3$ (14.34–17.60 wt.%) and low $TiO_2$ (0.4–2.73 wt.%). The $K_2O/Na_2O$ of AFS-1 samples ($SiO_2$ ~58 wt.%) are around 1 whereas these values range from 0.31 to 0.64 (average value is 0.43) in AFS-2 samples having low $SiO_2$ values (47.97–49.64 wt.%). When trace elements are taken into consideration, AFS-1 samples fall in the 'high potassic' and 'shonshonite' fields in the Th vs. Co diagram (Fig. 10A). In addition to this, the Ce/Yb vs. Ta/Yb (Fig. 10B) and Th/Yb vs. Ta/Yb (Fig. 10C) plots of AFS-1 samples clearly bring out their shoshonite affinity.

According to Müller et al. (1992), potassic volcanic rocks such as shoshonites, are an important constituent of volcanic suites in five main tectonic settings: (i) continental arcs, (ii) postcollisional arcs, (iii) initial oceanic arcs, (iv) late oceanic arcs, and (v) within-plate. Concentrations of most LILE, LREE and HFSE, and ratios such as Zr/A1 and Ti/A1, tend to be highest in Within-Plate potassic volcanic rocks, intermediate in Continental and Postcollisional Arc potassic volcanic rocks and lowest in Oceanic Arc potassic volcanic rocks. Postcollisional potassic volcanic rocks can be distinguished from Continental Arc potassic volcanic rocks by their higher Ce/P,

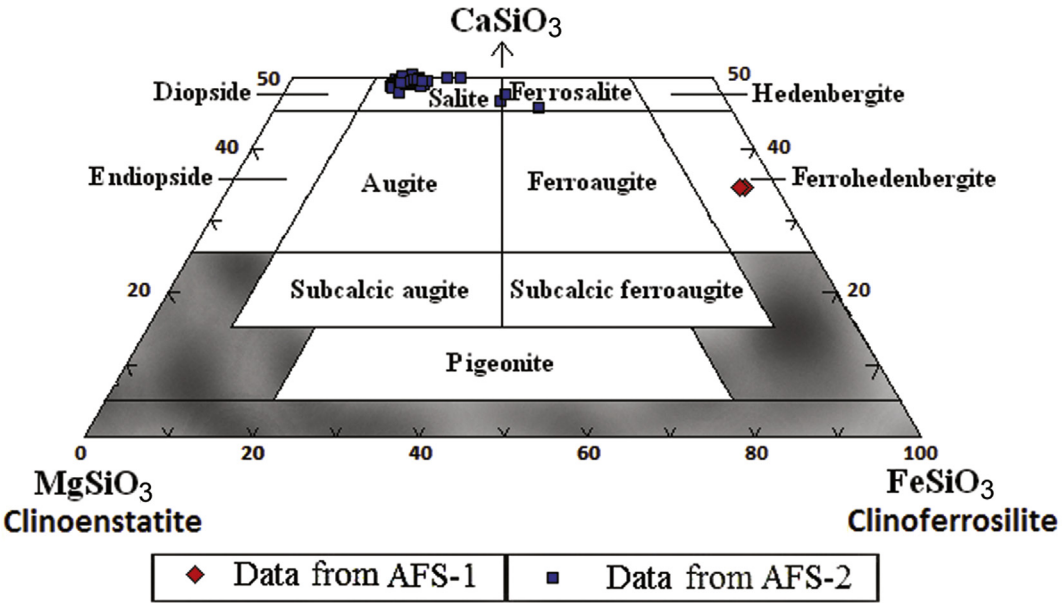


**Figure 7.** Pyroxene mineral composition in the pyroxene quadrilateral.

and lower Zr/Ce, Ti/Nb ratios. However, exact ratios by which the demarcations can be done are not known. Significant depletion of Ta-Nb-Ti in the multi-element normalized diagram along with enrichment of LILE and LREE are characteristic features of shoshonitic rocks formed in the arc settings. Alkali feldspar syenite from the present study are clearly devoid of negative Ta-Nb anomalies in the multi-element normalized diagram (Fig. 11) negating arc setting for these rocks. Shoshonite from the oceanic within-plate settings shows typical OIB type geochemical characteristics whereas the shoshonite from continental within-plate settings may exhibit either arc-type geochemical features (Wyborn, 1992; Leat et al., 1998) or OIB type features (Rogers et al., 1998). According to Müller et al. (1992), samples with $TiO_2$ above 1.5 wt.%, Zr above 350 ppm or Hf above 10 ppm may be considered with particular confidence as Within-Plate types. In the present study, slightly higher $TiO_2$ (0.35–2.73 wt.%), high Zr (614–1923 ppm) and Hf (18–26 ppm) concentrations likely point towards 'within-plate' setting.

According to Zhang et al. (2008), partial melting of either garnet or spinel peridotite will preferentially enrich the LREE such as La, which are more incompatible in most mantle phases than MREE such as Sm. However, the degree of enrichment of MREE relative to heavy REE such as Yb depends greatly on whether garnet exists as a residual phase during melting, because the heavy REE are preferentially retained by garnet during melting, but not by most other mantle phases. Furthermore, fractional crystallization will produce only modest changes in La/Sm and Sm/Yb ratios compared with variations caused by changes in melt fraction or source mineralogy. Large changes in La/Sm and Sm/Yb ratios remain almost constant during melting in the spinel stability field, whereas melting in the garnet stability field produces large changes in Sm/Yb ratios (Zhang et al., 2008). In the present case, variable La/Sm (8.6–16.3) and almost constant Sm/Yb (3.7–6.8) ratios indicate a spinel stability field for the alkali feldspar syenites studied here.

Crustal contamination which is an important process in the modification of any magma (DePaolo, 1981; Thompson et al., 1982; Dostal and Dupuy, 1984) can very well be evaluated by isotopic data and also by the trace element geochemistry. The multi-element spider diagram of crustally contaminated magma exhibits negative Nb and positive La-Th peaks. Thompson et al. (1984) pointed out that fusible crustal rock types are generally much richer in Ba, Rb, Th, K and light REE, but have similar or lower concentrations of Nb, Ta, P, Zr, Hf, Y and middle REE. In the present case, even though, positive Th and negative P anomaly are noticeable in the multi-element mantle normalized diagram (Fig. 11), the characteristic enrichment or depletion in the elemental concentrations which depicts crustal contamination (mainly negative Nb anomaly) is not noticeable. Scarrow et al. (2009) while discussing shoshonites, vaugnerites and potassic lamprophyres pointed out that crustal contamination will be better reflected in trace element

**Table 4**
Mineral chemical analyses of magnetite from AFS-1.

| | 1 | 2 | 3 |
|---|---|---|---|
| $SiO_2$ | 0.02 | 0.10 | 0.13 |
| $TiO_2$ | 13.00 | 11.04 | 8.41 |
| $Al_2O_3$ | 0.95 | 0.53 | 0.57 |
| $Cr_2O_3$ | 0.00 | 0.05 | 0.01 |
| FeO | 72.95 | 74.40 | 77.81 |
| MnO | 1.26 | 1.37 | 1.21 |
| MgO | 0.04 | 0.00 | 0.00 |
| CaO | 0.01 | 0.04 | 0.02 |
| $Na_2O$ | 0.00 | 0.00 | 0.01 |
| $K_2O$ | 0.01 | 0.00 | 0.00 |
| ZnO | 0.26 | 0.08 | 0.37 |
| $P_2O_5$ | 0.00 | 0.02 | 0.00 |
| Total | 88.49 | 87.64 | 88.54 |
| Formula (on the basis of 4 oxygen) | | | |
| Si | 0.001 | 0.005 | 0.007 |
| Ti | 0.468 | 0.409 | 0.315 |
| Al | 0.054 | 0.031 | 0.034 |
| Cr | 0.000 | 0.002 | 0.000 |
| Fe | 2.919 | 3.062 | 3.240 |
| Mn | 0.051 | 0.057 | 0.051 |
| Mg | 0.003 | 0.000 | 0.000 |
| Ca | 0.001 | 0.002 | 0.001 |
| Na | 0.000 | 0.000 | 0.001 |
| K | 0.001 | 0.000 | 0.000 |
| Zn | 0.009 | 0.003 | 0.014 |
| P | 0.000 | 0.001 | 0.000 |

**Table 5**
Mineral chemical analyses of pyroxene from AFS-2. R = rim and C = core.

| | 1C | 2R | 3R | 4C | 5R | 6R | 7C | 8R | 9C | 10C | 11C | 12C | 13R |
|---|---|---|---|---|---|---|---|---|---|---|---|---|---|
| $SiO_2$ | 51.37 | 51.73 | 49.65 | 48.84 | 51.24 | 50.14 | 51.86 | 51.59 | 52.35 | 51.79 | 50.82 | 52.20 | 50.63 |
| $TiO_2$ | 1.37 | 1.49 | 1.77 | 2.34 | 1.47 | 1.41 | 1.36 | 1.30 | 1.47 | 1.39 | 1.46 | 1.39 | 1.42 |
| $Al_2O_3$ | 3.06 | 3.00 | 3.97 | 4.49 | 3.24 | 3.68 | 3.02 | 2.50 | 3.32 | 3.08 | 3.35 | 3.03 | 3.09 |
| $Cr_2O_3$ | 0.01 | 0.01 | 0.02 | 0.00 | 0.00 | 0.01 | 0.00 | 0.01 | 0.01 | 0.01 | 0.00 | 0.00 | 0.00 |
| FeO | 7.49 | 8.54 | 10.74 | 8.01 | 9.42 | 11.35 | 7.42 | 8.27 | 7.68 | 7.59 | 7.56 | 7.45 | 9.53 |
| MnO | 0.11 | 0.23 | 0.27 | 0.13 | 0.27 | 0.31 | 0.09 | 0.23 | 0.11 | 0.07 | 0.12 | 0.09 | 0.25 |
| MgO | 13.56 | 12.56 | 10.79 | 12.22 | 11.73 | 9.97 | 12.92 | 12.05 | 13.20 | 12.97 | 12.92 | 13.52 | 11.63 |
| CaO | 23.79 | 23.84 | 23.47 | 22.61 | 22.86 | 22.77 | 23.57 | 23.65 | 23.59 | 23.25 | 23.20 | 23.50 | 23.24 |
| $Na_2O$ | 0.89 | 0.96 | 1.07 | 0.99 | 1.20 | 1.23 | 0.82 | 0.91 | 0.85 | 0.85 | 0.82 | 0.84 | 1.12 |
| $K_2O$ | 0.00 | 0.00 | 0.00 | 0.00 | 0.00 | 0.00 | 0.01 | 0.00 | 0.00 | 0.00 | 0.01 | 0.00 | 0.00 |
| NiO | 0.00 | 0.00 | 0.00 | 0.00 | 0.00 | 0.02 | 0.00 | 0.00 | 0.00 | 0.05 | 0.00 | 0.00 | 0.05 |
| Total | **101.65** | **102.35** | **101.76** | **99.61** | **101.42** | **100.89** | **101.07** | **100.52** | **102.57** | **101.04** | **100.25** | **102.03** | **100.96** |
| Formula (on the basis of 6 oxygen) | | | | | | | | | | | | | |
| Si | 1.889 | 1.898 | 1.856 | 1.839 | 1.902 | 1.890 | 1.912 | 1.924 | 1.903 | 1.911 | 1.893 | 1.906 | 1.894 |
| Ti | 0.038 | 0.041 | 0.050 | 0.066 | 0.041 | 0.040 | 0.038 | 0.037 | 0.040 | 0.038 | 0.041 | 0.038 | 0.040 |
| Al | 0.133 | 0.130 | 0.176 | 0.200 | 0.142 | 0.164 | 0.132 | 0.111 | 0.143 | 0.134 | 0.148 | 0.131 | 0.137 |
| Cr | 0.000 | 0.000 | 0.000 | 0.000 | 0.000 | 0.000 | 0.000 | 0.000 | 0.000 | 0.000 | 0.000 | 0.000 | 0.000 |
| Fe | 0.230 | 0.262 | 0.336 | 0.252 | 0.292 | 0.358 | 0.229 | 0.258 | 0.233 | 0.234 | 0.236 | 0.228 | 0.298 |
| Mn | 0.004 | 0.007 | 0.009 | 0.004 | 0.008 | 0.010 | 0.003 | 0.007 | 0.003 | 0.002 | 0.004 | 0.003 | 0.008 |
| Mg | 0.743 | 0.687 | 0.601 | 0.686 | 0.649 | 0.560 | 0.710 | 0.670 | 0.715 | 0.713 | 0.717 | 0.736 | 0.649 |
| Ca | 0.938 | 0.937 | 0.940 | 0.912 | 0.909 | 0.920 | 0.931 | 0.945 | 0.919 | 0.919 | 0.926 | 0.919 | 0.932 |
| Na | 0.064 | 0.068 | 0.078 | 0.072 | 0.087 | 0.090 | 0.058 | 0.066 | 0.060 | 0.061 | 0.059 | 0.060 | 0.081 |
| K | 0.000 | 0.000 | 0.000 | 0.000 | 0.000 | 0.000 | 0.001 | 0.000 | 0.000 | 0.000 | 0.000 | 0.000 | 0.000 |
| Ni | 0.000 | 0.000 | 0.000 | 0.000 | 0.000 | 0.001 | 0.000 | 0.000 | 0.000 | 0.001 | 0.000 | 0.000 | 0.002 |
| Ca | 48.98 | 49.50 | 49.84 | 49.19 | 48.92 | 49.78 | 49.71 | 50.27 | 49.14 | 49.20 | 49.18 | 48.73 | 49.39 |
| Mg | 38.80 | 36.29 | 31.87 | 37.00 | 34.93 | 30.30 | 37.91 | 35.64 | 38.24 | 38.17 | 38.08 | 39.02 | 34.39 |
| Fe + Mn | 12.22 | 14.21 | 18.29 | 13.81 | 16.15 | 19.91 | 12.39 | 14.10 | 12.62 | 12.63 | 12.75 | 12.25 | 16.22 |

| | 14C | 15R | 16R | 17C | 18R | 19R | 20C | 21C | 22R |
|---|---|---|---|---|---|---|---|---|---|
| $SiO_2$ | 51.05 | 49.63 | 49.87 | 49.35 | 49.93 | 50.41 | 49.48 | 49.13 | 50.04 |
| $TiO_2$ | 1.43 | 1.88 | 1.47 | 1.94 | 1.67 | 1.37 | 1.57 | 1.64 | 0.57 |
| $Al_2O_3$ | 2.35 | 3.41 | 2.64 | 3.68 | 2.77 | 2.34 | 3.06 | 3.26 | 1.59 |
| $Cr_2O_3$ | 0.00 | 0.02 | 0.05 | 0.01 | 0.03 | 0.01 | 0.00 | 0.01 | 0.01 |
| FeO | 7.20 | 7.38 | 7.33 | 7.77 | 8.03 | 8.34 | 7.55 | 8.40 | 15.95 |
| MnO | 0.26 | 0.16 | 0.30 | 0.10 | 0.23 | 0.34 | 0.23 | 0.27 | 0.88 |
| MgO | 13.14 | 12.33 | 12.42 | 12.42 | 12.29 | 12.22 | 12.44 | 11.42 | 6.86 |
| CaO | 22.62 | 22.48 | 23.28 | 21.43 | 22.48 | 22.89 | 22.62 | 22.45 | 19.11 |
| $Na_2O$ | 0.67 | 0.80 | 0.81 | 0.82 | 0.79 | 0.81 | 0.93 | 1.04 | 2.24 |
| $K_2O$ | 0.00 | 0.00 | 0.02 | 0.00 | 0.02 | 0.01 | 0.00 | 0.00 | 0.02 |
| ZnO | 0.02 | 0.00 | 0.00 | 0.04 | 0.00 | 0.00 | 0.00 | 0.15 | 0.09 |
| $P_2O_5$ | 0.02 | 0.00 | 0.00 | 0.00 | 0.01 | 0.00 | 0.04 | 0.01 | 0.01 |
| Total | **98.75** | **98.08** | **98.18** | **97.56** | **98.26** | **98.75** | **97.91** | **97.79** | **97.36** |
| Formula (on the basis of 6 oxygen) | | | | | | | | | |
| Si | 1.925 | 1.888 | 1.902 | 1.886 | 1.903 | 1.916 | 1.892 | 1.890 | 1.991 |
| Ti | 0.041 | 0.054 | 0.042 | 0.056 | 0.048 | 0.039 | 0.045 | 0.048 | 0.017 |
| Al | 0.105 | 0.154 | 0.119 | 0.167 | 0.125 | 0.105 | 0.139 | 0.149 | 0.075 |
| Cr | 0.000 | 0.001 | 0.002 | 0.000 | 0.001 | 0.000 | 0.000 | 0.000 | 0.000 |
| Fe | 0.227 | 0.235 | 0.234 | 0.248 | 0.256 | 0.265 | 0.241 | 0.270 | 0.531 |
| Mn | 0.008 | 0.005 | 0.010 | 0.003 | 0.007 | 0.011 | 0.007 | 0.009 | 0.030 |
| Mg | 0.738 | 0.699 | 0.706 | 0.707 | 0.698 | 0.692 | 0.709 | 0.655 | 0.407 |
| Ca | 0.914 | 0.917 | 0.951 | 0.877 | 0.918 | 0.932 | 0.927 | 0.926 | 0.815 |
| Na | 0.049 | 0.059 | 0.060 | 0.061 | 0.058 | 0.060 | 0.069 | 0.078 | 0.173 |
| K | 0.000 | 0.000 | 0.001 | 0.000 | 0.001 | 0.001 | 0.000 | 0.000 | 0.001 |
| Zn | 0.001 | 0.000 | 0.000 | 0.001 | 0.000 | 0.000 | 0.000 | 0.004 | 0.003 |
| P | 0.001 | 0.000 | 0.000 | 0.000 | 0.000 | 0.000 | 0.001 | 0.000 | 0.000 |
| Ca | 48.44 | 49.44 | 50.03 | 47.79 | 48.86 | 49.05 | 49.20 | 49.79 | 45.71 |
| Mg | 39.11 | 37.66 | 37.14 | 38.53 | 37.15 | 36.42 | 37.63 | 35.22 | 22.83 |
| Fe + Mn | 12.45 | 12.93 | 12.84 | 13.68 | 14.00 | 14.53 | 13.16 | 15.00 | 31.46 |

| | 23C | 24C | 25R | 26C | 27C | 28C | 29C | 30R |
|---|---|---|---|---|---|---|---|---|
| $SiO_2$ | 48.38 | 50.77 | 49.59 | 48.57 | 48.78 | 46.97 | 47.96 | 47.88 |
| $TiO_2$ | 2.11 | 1.19 | 0.82 | 2.06 | 1.54 | 2.84 | 2.56 | 1.12 |
| $Al_2O_3$ | 4.05 | 2.08 | 3.35 | 4.07 | 3.14 | 4.09 | 4.18 | 4.62 |
| $Cr_2O_3$ | 0.00 | 0.00 | 0.00 | 0.03 | 0.00 | 0.03 | 0.00 | 0.05 |
| FeO | 8.10 | 8.14 | 13.63 | 8.02 | 8.92 | 8.41 | 8.81 | 13.45 |
| MnO | 0.28 | 0.28 | 0.64 | 0.34 | 0.28 | 0.20 | 0.29 | 0.64 |
| MgO | 11.77 | 12.01 | 8.19 | 11.46 | 11.65 | 11.51 | 11.35 | 7.80 |
| CaO | 22.08 | 22.83 | 19.62 | 22.17 | 22.32 | 22.46 | 22.30 | 19.89 |
| $Na_2O$ | 0.97 | 0.90 | 2.42 | 1.05 | 1.12 | 0.80 | 0.86 | 2.13 |
| $K_2O$ | 0.03 | 0.01 | 0.02 | 0.00 | 0.02 | 0.02 | 0.00 | 0.02 |
| ZnO | 0.19 | 0.00 | 0.04 | 0.00 | 0.04 | 0.00 | 0.01 | 0.09 |
| $P_2O_5$ | 0.07 | 0.01 | 0.04 | 0.04 | 0.01 | 0.03 | 0.06 | 0.00 |
| Total | 98.03 | **98.21** | **98.34** | **97.82** | **97.83** | **97.38** | **98.39** | **97.69** |
| Formula (on the basis of 6 oxygen) | | | | | | | | |
| Si | 1.856 | 1.937 | 1.933 | 1.864 | 1.882 | 1.822 | 1.84 | 1.883 |

**Table 5** (*continued*)

| | 23C | 24C | 25R | 26C | 27C | 28C | 29C | 30R |
|---|---|---|---|---|---|---|---|---|
| Ti | 0.061 | 0.034 | 0.024 | 0.06 | 0.045 | 0.083 | 0.074 | 0.033 |
| Al | 0.184 | 0.094 | 0.155 | 0.185 | 0.144 | 0.188 | 0.19 | 0.215 |
| Cr | 0.000 | 0.000 | 0.000 | 0.001 | 0.000 | 0.001 | 0.000 | 0.002 |
| Fe | 0.260 | 0.260 | 0.444 | 0.257 | 0.288 | 0.273 | 0.283 | 0.442 |
| Mn | 0.009 | 0.009 | 0.021 | 0.011 | 0.009 | 0.007 | 0.009 | 0.021 |
| Mg | 0.673 | 0.683 | 0.476 | 0.656 | 0.670 | 0.665 | 0.649 | 0.457 |
| Ca | 0.908 | 0.933 | 0.820 | 0.912 | 0.923 | 0.934 | 0.917 | 0.838 |
| Na | 0.072 | 0.067 | 0.183 | 0.078 | 0.084 | 0.060 | 0.064 | 0.162 |
| K | 0.002 | 0.001 | 0.001 | 0.000 | 0.001 | 0.001 | 0.000 | 0.001 |
| Zn | 0.005 | 0.000 | 0.001 | 0.000 | 0.001 | 0.000 | 0.000 | 0.003 |
| P | 0.002 | 0.000 | 0.001 | 0.001 | 0.000 | 0.001 | 0.002 | 0.000 |
| Ca | 49.08 | 49.50 | 46.57 | 49.67 | 48.84 | 49.71 | 49.35 | 47.67 |
| Mg | 36.38 | 36.23 | 27.03 | 35.73 | 35.45 | 35.39 | 34.93 | 26.00 |
| Fe + Mn | 14.54 | 14.27 | 26.41 | 14.60 | 15.71 | 14.90 | 15.72 | 26.34 |

geochemistry. They opined that melts derived from old metasomatised mantle with little crustal contamination are reflected by their mantle like Th/U ratio, low Cs (<5 ppm) and high Rb/Cs (>40). In the present case, the geochemical data of AFS-1 exhibit high Rb/Cs (48–54) and low Cs (4–5 ppm) (Table 10). Zhang et al. (2008) pointed out that low Th/Ce ratios and absence of negative Eu anomalies suggest that crustal contamination does not play a significant role in the modification of magmas because continental crust has relatively high Th/Ce ratios (~0.15) and negative Eu anomalies (Taylor and McLennan, 1995), while mantle-derived magmas have low Th/Ce ratios (0.02–0.05, Sun and McDonough, 1989). The absence of negative Eu anomaly as well as low Th/Ce ratios (0.11–0.13) of alkali feldspar syenites in the present study, further substantiate that crustal contamination was not a major process in the magma modification.

Li et al. (2000), while discussing the petogenesis of shoshonites from SE Guangxi, pointed out that within-plate potassic magma is

**Table 6**
Mineral chemical analyses of feldspar from AFS-2.

| | 1 | 2 | 3 | 4 | 5 |
|---|---|---|---|---|---|
| $SiO_2$ | 63.19 | 63.63 | 63.44 | 63.09 | 62.35 |
| $TiO_2$ | 0.65 | 0.19 | 0.05 | 0.02 | 0.10 |
| $Al_2O_3$ | 16.23 | 17.51 | 17.90 | 17.67 | 24.29 |
| $Cr_2O_3$ | 0.00 | 0.00 | 0.02 | 0.00 | 0.00 |
| FeO | 2.34 | 0.57 | 0.74 | 0.40 | 0.79 |
| MnO | 0.00 | 0.03 | 0.08 | 0.00 | 0.03 |
| MgO | 0.04 | 0.01 | 0.07 | 0.01 | 0.00 |
| CaO | 0.92 | 0.10 | 0.00 | 0.00 | 0.07 |
| $Na_2O$ | 0.24 | 0.14 | 0.12 | 0.08 | 8.20 |
| $K_2O$ | 15.34 | 15.87 | 16.16 | 15.97 | 0.17 |
| ZnO | 0.06 | 0.00 | 0.04 | 0.07 | 0.00 |
| $P_2O_5$ | 0.03 | 0.00 | 0.00 | 0.00 | 0.00 |
| Total | **99.06** | **98.05** | **98.62** | **97.30** | **96.01** |
| Formula (on the basis of 32 oxygen) | | | | | |
| Si | 11.956 | 12.020 | 11.950 | 12.008 | 11.296 |
| Ti | 0.093 | 0.027 | 0.007 | 0.003 | 0.014 |
| Al | 3.639 | 3.919 | 3.995 | 3.985 | 5.214 |
| Cr | 0.000 | 0.000 | 0.003 | 0.000 | 0.000 |
| Fe | 0.370 | 0.090 | 0.117 | 0.064 | 0.120 |
| Mn | 0.000 | 0.005 | 0.013 | 0.000 | 0.005 |
| Mg | 0.011 | 0.003 | 0.020 | 0.003 | 0.000 |
| Ca | 0.187 | 0.020 | 0.000 | 0.000 | 0.014 |
| Na | 0.088 | 0.051 | 0.044 | 0.030 | 2.881 |
| K | 3.703 | 3.825 | 3.884 | 3.878 | 0.039 |
| Zn | 0.008 | 0.000 | 0.006 | 0.010 | 0.000 |
| P | 0.005 | 0.000 | 0.000 | 0.000 | 0.000 |
| Or | 93.09 | 98.18 | 98.88 | 99.23 | 1.33 |
| Ab | 2.21 | 1.31 | 1.12 | 0.77 | 98.19 |
| An | 4.70 | 0.51 | 0.00 | 0.00 | 0.48 |

**Table 7**
Mineral chemical analyses of titanite from AFS-2.

| | 1 |
|---|---|
| $SiO_2$ | 30.80 |
| $TiO_2$ | 37.25 |
| $Al_2O_3$ | 0.46 |
| $Cr_2O_3$ | 0.00 |
| FeO | 1.75 |
| MnO | 0.05 |
| MgO | 0.04 |
| CaO | 28.18 |
| $Na_2O$ | 0.05 |
| $K_2O$ | 0.01 |
| Total | **98.60** |
| Formula (on the basis of 20 oxygen) | |
| Si | 4.100 |
| Ti | 3.728 |
| Al | 0.072 |
| Cr | 0.000 |
| Fe | 0.194 |
| Mn | 0.006 |
| Mg | 0.008 |
| Ca | 4.019 |
| Na | 0.014 |
| K | 0.002 |

**Table 8**
Mineral chemical analyses of magnetite from AFS-2.

| | 1 | 2 |
|---|---|---|
| $SiO_2$ | 0.098 | 0.956 |
| $TiO_2$ | 13.867 | 14.103 |
| $Al_2O_3$ | 0.768 | 1.007 |
| $Cr_2O_3$ | 0.015 | 0.024 |
| FeO | 76.293 | 75.949 |
| MnO | 1.140 | 1.387 |
| MgO | 1.137 | 1.213 |
| CaO | 0.148 | 0.113 |
| $Na_2O$ | 0.006 | 0.423 |
| $K_2O$ | 0.000 | 0.031 |
| NiO | 0.000 | 0.001 |
| Total | 93.473 | 95.205 |
| Formula (on the basis of 4 oxygen) | | |
| Si | 0.004 | 0.042 |
| Ti | 0.468 | 0.461 |
| Al | 0.041 | 0.052 |
| Cr | 0.001 | 0.001 |
| Fe | 2.866 | 2.762 |
| Mn | 0.043 | 0.051 |
| Mg | 0.076 | 0.079 |
| Ca | 0.007 | 0.005 |
| Na | 0.001 | 0.036 |
| K | 0.000 | 0.002 |
| Ni | 0.000 | 0.000 |

**Table 9**
Major element analysis in wt.% along with CIPW norms. AFS-1 → GR-2A, GR-2B, GR-2C and GR-2D; AFS-2 → U-12A, U-12B, U-12C, U-12D, U-13A, U-13B, U-13C and U-13D.

| Sample | AFS-1 | | | | AFS-2 | | | | | | | |
|---|---|---|---|---|---|---|---|---|---|---|---|---|
| | GR-2A | GR-2B | GR-2C | GR-2D | U-12A | U-12B | U-12C | U-12D | U-13A | U-13B | U-13C | U-13D |
| $SiO_2$ | 58.03 | 58.80 | 58.70 | 58.59 | 49.09 | 49.03 | 47.97 | 48.02 | 48.74 | 49.12 | 48.98 | 49.64 |
| $TiO_2$ | 0.40 | 0.40 | 0.40 | 0.35 | 2.68 | 2.68 | 2.60 | 2.73 | 2.45 | 2.50 | 2.63 | 2.60 |
| $Al_2O_3$ | 17.60 | 17.48 | 17.45 | 17.41 | 15.14 | 15.07 | 15.07 | 15.06 | 14.34 | 14.38 | 14.78 | 14.89 |
| $Fe_2O_3$ | 7.51 | 7.51 | 7.48 | 7.43 | 9.90 | 9.91 | 9.18 | 9.45 | 8.89 | 9.06 | 9.60 | 9.15 |
| MnO | 0.16 | 0.15 | 0.15 | 0.12 | 0.26 | 0.26 | 0.25 | 0.26 | 0.24 | 0.25 | 0.25 | 0.24 |
| MgO | 1.73 | 1.73 | 1.72 | 0.41 | 4.45 | 4.46 | 4.33 | 4.23 | 4.40 | 4.48 | 4.25 | 4.18 |
| CaO | 2.97 | 2.97 | 2.95 | 2.15 | 7.61 | 7.69 | 7.22 | 7.66 | 9.95 | 10.07 | 7.79 | 7.98 |
| $Na_2O$ | 4.87 | 4.79 | 4.63 | 6.32 | 7.11 | 7.12 | 7.59 | 7.67 | 5.32 | 5.31 | 7.54 | 6.78 |
| $K_2O$ | 4.75 | 4.75 | 4.73 | 5.91 | 3.01 | 3.01 | 3.27 | 2.90 | 3.41 | 3.42 | 2.33 | 3.17 |
| $P_2O_5$ | 0.10 | 0.10 | 0.09 | 0.12 | 0.89 | 0.92 | 0.81 | 0.87 | 0.98 | 0.96 | 0.80 | 0.83 |
| Sum | 98.12 | 98.68 | 98.30 | 98.81 | 100.14 | 100.14 | 98.28 | 98.83 | 98.73 | 99.54 | 98.95 | 99.46 |
| CIPW NORMS | | | | | | | | | | | | |
| Q | 3.28 | 4.51 | 5.29 | 0.00 | 0.00 | 0.00 | 0.00 | 0.00 | 0.00 | 0.00 | 0.00 | 0.00 |
| Or | 28.07 | 28.07 | 27.95 | 34.93 | 17.76 | 17.77 | 19.31 | 17.12 | 20.16 | 20.19 | 13.78 | 18.72 |
| Ab | 41.21 | 40.53 | 39.18 | 45.32 | 27.85 | 27.60 | 19.89 | 22.60 | 22.02 | 22.25 | 30.37 | 27.76 |
| An | 12.13 | 12.17 | 12.86 | 1.68 | 0.52 | 0.31 | 0.00 | 0.00 | 5.21 | 5.29 | 0.00 | 0.80 |
| Ne | 0.00 | 0.00 | 0.00 | 4.42 | 17.51 | 17.67 | 21.35 | 20.98 | 12.44 | 12.30 | 17.69 | 16.06 |
| Di | 0.92 | 0.87 | 0.30 | 2.21 | 18.03 | 18.36 | 17.55 | 18.59 | 23.50 | 23.88 | 19.70 | 19.68 |
| Hy | 3.88 | 3.91 | 4.15 | 0.00 | 0.00 | 0.00 | 0.00 | 0.00 | 0.00 | 0.00 | 0.00 | 0.00 |
| Ol | 0.00 | 0.00 | 0.00 | 0.00 | 1.93 | 1.83 | 1.87 | 1.35 | 0.06 | 0.07 | 1.04 | 0.91 |
| Il | 0.34 | 0.32 | 0.32 | 0.26 | 0.55 | 0.55 | 0.53 | 0.55 | 0.52 | 0.53 | 0.54 | 0.52 |
| Ap | 0.23 | 0.23 | 0.21 | 0.28 | 2.05 | 2.12 | 1.88 | 2.01 | 2.28 | 2.23 | 1.85 | 1.93 |
| Ac | 0.00 | 0.00 | 0.00 | 0.00 | 0.00 | 0.00 | 4.31 | 3.18 | 0.00 | 0.00 | 0.67 | 0.00 |
| Wo | 0.00 | 0.00 | 0.00 | 1.93 | 0.00 | 0.00 | 0.00 | 0.00 | 0.00 | 0.00 | 0.00 | 0.00 |
| Hm | 7.51 | 7.51 | 7.48 | 7.43 | 9.90 | 9.91 | 7.69 | 8.35 | 8.89 | 9.06 | 9.37 | 9.15 |
| Tn | 0.54 | 0.57 | 0.57 | 0.00 | 0.00 | 0.00 | 0.00 | 0.00 | 0.00 | 0.00 | 0.00 | 0.00 |
| Pf | 0.00 | 0.00 | 0.00 | 0.37 | 4.08 | 4.07 | 3.94 | 4.15 | 3.71 | 3.78 | 3.99 | 3.96 |
| Peralkaline index | 0.75 | 0.74 | 0.73 | 0.96 | 0.99 | 0.99 | 1.06 | 1.05 | 0.87 | 0.87 | 1.01 | 0.98 |
| $K_2O/Na_2O$ | 0.98 | 0.99 | 1.02 | 0.94 | 0.42 | 0.42 | 0.43 | 0.38 | 0.64 | 0.64 | 0.31 | 0.47 |

**Table 10**
Trace element analysis in ppm. AFS-1 → GR-2A, GR-2B, GR-2C & GR-2D; AFS-2 → U-12A, U-12B, U-12C, U-12D, U-13A, U-13B, U-13C& U-13D. n.d. → not determined.

| Sample | AFS-1 | | | | AFS-2 | | | | | | | |
|---|---|---|---|---|---|---|---|---|---|---|---|---|
| | GR-2A | GR-2B | GR-2C | GR-2D | U-12A | U-12B | U-12C | U-12D | U-13A | U-13B | U-13C | U-13D |
| Sc | 5.81 | 6.21 | 4.90 | 5.24 | **n.d.** | **n.d.** | **n.d.** | **n.d.** | **n.d.** | **n.d.** | **n.d.** | **n.d.** |
| V | 42.83 | 48.24 | 37.74 | 37.04 | 289.00 | 281.00 | 275.00 | 299.00 | 232.00 | 248.00 | 314.00 | 301.00 |
| Cr | 96.92 | 164.74 | 129.92 | 163.40 | 5.00 | 5.00 | 13.00 | 13.00 | 4.00 | 5.00 | 20.00 | 11.00 |
| Co | 5.77 | 6.07 | 5.27 | 5.46 | 34.00 | 33.00 | 29.00 | 32.00 | 30.00 | 31.00 | 29.00 | 31.00 |
| Ni | 11.39 | 58.20 | 16.17 | 76.90 | 5.30 | 3.90 | 7.50 | 7.30 | 6.30 | 5.60 | 6.70 | 8.80 |
| Cu | 23.35 | 28.52 | 24.59 | 30.30 | **n.d.** | **n.d.** | **n.d.** | **n.d.** | **n.d.** | **n.d.** | **n.d.** | **n.d.** |
| Zn | 76.26 | 97.23 | 88.16 | 98.93 | **n.d.** | **n.d.** | **n.d.** | **n.d.** | **n.d.** | **n.d.** | **n.d.** | **n.d.** |
| Ga | 23.60 | 29.04 | 26.23 | 25.97 | **n.d.** | **n.d.** | **n.d.** | **n.d.** | **n.d.** | **n.d.** | **n.d.** | **n.d.** |
| Rb | 214.0 | 254.4 | 240.1 | 231.6 | 69.6 | 67.9 | 67.5 | 75.0 | 77.4 | 75.8 | 61.2 | 65.5 |
| Sr | 417.0 | 480.0 | 441.3 | 433.6 | 2182 | 2171 | 2303 | 2160 | 2858 | 2846 | 2369 | 2962 |
| Y | 47.5 | 56.8 | 52.2 | 50.3 | 50.4 | 50.9 | 48.8 | 51.5 | 51.2 | 52.4 | 48.8 | 49.7 |
| Zr | 890.47 | 1269.46 | 1923.07 | 1073.49 | 713.00 | 709.00 | 706.00 | 753.00 | 614.00 | 617.00 | 693.00 | 618.00 |
| Nb | 277.20 | 312.69 | 291.88 | 283.08 | 238.60 | 236.40 | 239.70 | 248.20 | 243.90 | 244.50 | 236.70 | 240.80 |
| Cs | 4.0 | 5.0 | 5.0 | 5.0 | **n.d.** | **n.d.** | **n.d.** | **n.d.** | **n.d.** | **n.d.** | **n.d.** | **n.d.** |
| Ba | 564.7 | 686.0 | 669.1 | 658.2 | 1861.0 | 1850.0 | 2105.0 | 1935.0 | 2215.0 | 2259.0 | 1791.0 | 1916.0 |
| La | 200.78 | 238.51 | 223.74 | 223.52 | 217.00 | 233.00 | 229.00 | 231.00 | 237.00 | 247.00 | 219.00 | 225.00 |
| Ce | 310.53 | 361.32 | 344.92 | 339.76 | 425.00 | 465.00 | 426.00 | 447.00 | 461.00 | 482.00 | 420.00 | 432.00 |
| Pr | 27.10 | 31.07 | 29.91 | 29.36 | 47.00 | 48.00 | 45.50 | 51.00 | 51.00 | 51.34 | 47.00 | 49.00 |
| Nd | 98.80 | 113.82 | 109.75 | 107.98 | 171.00 | 187.00 | 184.00 | 183.00 | 184.00 | 192.00 | 168.00 | 169.00 |
| Sm | 12.93 | 14.60 | 14.46 | 14.17 | 26.00 | 25.71 | 24.13 | 26.64 | 26.95 | 27.63 | 25.50 | 25.90 |
| Eu | 3.77 | 4.58 | 4.41 | 4.33 | 6.96 | 6.88 | 6.43 | 7.40 | 7.15 | 7.31 | 6.70 | 7.20 |
| Gd | 16.52 | 18.75 | 17.99 | 17.59 | 22.42 | 22.10 | 21.20 | 22.70 | 22.94 | 23.76 | 21.80 | 21.90 |
| Tb | 1.43 | 1.67 | 1.64 | 1.55 | 2.58 | 2.62 | 2.50 | 2.67 | 2.70 | 2.77 | 2.55 | 2.52 |
| Dy | 7.24 | 8.62 | 8.36 | 8.15 | 11.23 | 11.50 | 11.10 | 12.15 | 12.10 | 12.27 | 11.20 | 11.50 |
| Ho | 1.51 | 1.82 | 1.79 | 1.72 | 1.98 | 2.00 | 1.91 | 2.14 | 2.06 | 2.08 | 1.98 | 2.04 |
| Er | 4. 60 | 5.49 | 5.51 | 5.26 | 4.90 | 4.94 | 4.67 | 5.30 | 5.10 | 5.33 | 4.95 | 4.95 |
| Tm | 0.51 | 0.62 | 0.61 | 0.59 | 0.62 | 0.64 | 0.60 | 0.68 | 0.63 | 0.66 | 0.62 | 0.66 |
| Yb | 3.21 | 3.84 | 3.93 | 3.78 | 3.82 | 3.92 | 3.80 | 4.10 | 4.02 | 4.09 | 3.88 | 3.90 |
| Lu | 0.71 | 0.86 | 0.90 | 0.83 | 0.57 | 0.55 | 0.53 | 0.60 | 0.56 | 0.59 | 0.56 | 0.56 |
| Hf | 18.35 | 26.63 | 26.40 | 24.30 | **n.d.** | **n.d.** | **n.d.** | **n.d.** | **n.d.** | **n.d.** | **n.d.** | **n.d.** |
| Ta | 17.07 | 16.80 | 16.89 | 17.71 | **n.d.** | **n.d.** | **n.d.** | **n.d.** | **n.d.** | **n.d.** | **n.d.** | **n.d.** |
| Pb | 4.18 | 5.67 | 5.79 | 6.24 | **n.d.** | **n.d.** | **n.d.** | **n.d.** | **n.d.** | **n.d.** | **n.d.** | **n.d.** |
| Th | 34. 5 | 41.8 | 42.9 | 42.4 | **n.d.** | **n.d.** | **n.d.** | **n.d.** | **n.d.** | **n.d.** | **n.d.** | **n.d.** |
| U | 4.2 | 5.5 | 5.6 | 5.7 | **n.d.** | **n.d.** | **n.d.** | **n.d.** | **n.d.** | **n.d.** | **n.d.** | **n.d.** |
| ∑REE | 689 | 805 | 767 | 758 | 941 | 1013 | 961 | 996 | 1017 | 1058 | 933 | 956 |
| La/Yb | 62.59 | 62.10 | 57.00 | 59.10 | 56.81 | 59.44 | 60.26 | 56.34 | 58.96 | 60.39 | 56.44 | 57.69 |
| La/Sm | 15.53 | 16.34 | 15.47 | 15.77 | 8.35 | 9.06 | 9.49 | 8.67 | 8.79 | 8.94 | 8.59 | 8.69 |
| Zr/Sm | 68.89 | 86.94 | 132.99 | 75.75 | 27.43 | 27.59 | 29.27 | 28.25 | 22.79 | 22.32 | 27.17 | 23.86 |
| Sm/Yb | 4.03 | 3.80 | 3.68 | 3.75 | 6.81 | 6.56 | 6.35 | 6.50 | 6.70 | 6.76 | 6.57 | 6.64 |
| Th/Ce | 0.11 | 0.12 | 0.13 | 0.13 | **n.d.** | **n.d.** | **n.d.** | **n.d.** | **n.d.** | **n.d.** | **n.d.** | **n.d.** |
| Rb/Cs | 54.02 | 51.19 | 49.19 | 48.57 | **n.d.** | **n.d.** | **n.d.** | **n.d.** | **n.d.** | **n.d.** | **n.d.** | **n.d.** |

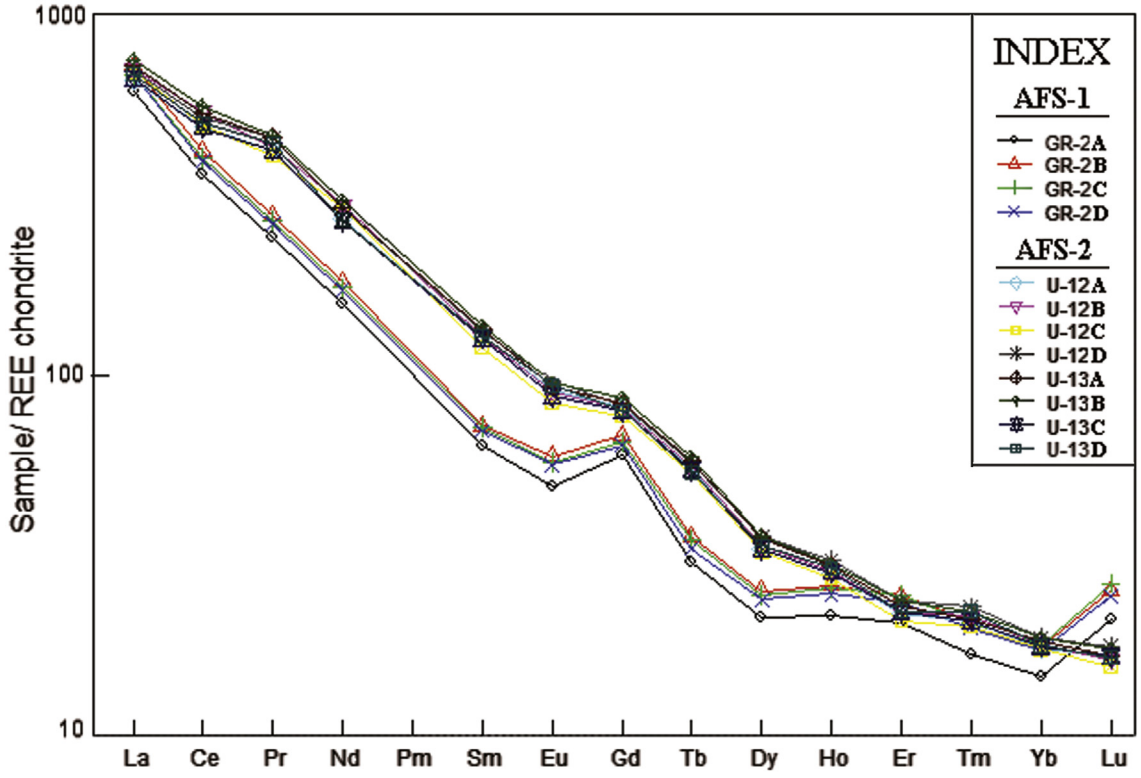


**Figure 8.** Chondrite-normalized (after Nakamura, 1974) REE distribution patterns for alkali feldspar syenites from the Chhotaudepur province.

commonly generated during thinning of the lithosphere and upwelling of the asthenosphere, and LILE enrichment within the lithosphere may result from metasomatism of under plating of plume induced magma, or the long term heterogeneity of the lithosphere. In the present case, the enrichment of LILE and LREE, and the absence of Nb depletion clearly point to a within-plate and rifting environment. Similar type of geochemical features in shoshonitic rocks from within-plate and rifting environments have recently been reported from China (Li et al., 2000; Deng et al., 2012).

Various hypotheses have been put forward by different workers on the origin of syenite and associated rocks around the world which include (i) partial melting of lithospheric mantle that was enriched by subduction (Rios et al., 2007; West et al., 2007; Lan et al., 2011; Rajesh et al., 2013), (ii) melting of the sources which might have been metasomatized by OIB type melts in an intraplate regime (Li et al., 2000; Rajesh et al., 2013), (iii) partial melting of metasomatized/enriched mantle (Currie, 1989; Litvinovsky et al., 2002; Miyazaki et al., 2003; Conceição and Green, 2004; Wang et al., 2005), (iv) differentiation of alkali basalt magma (Brown

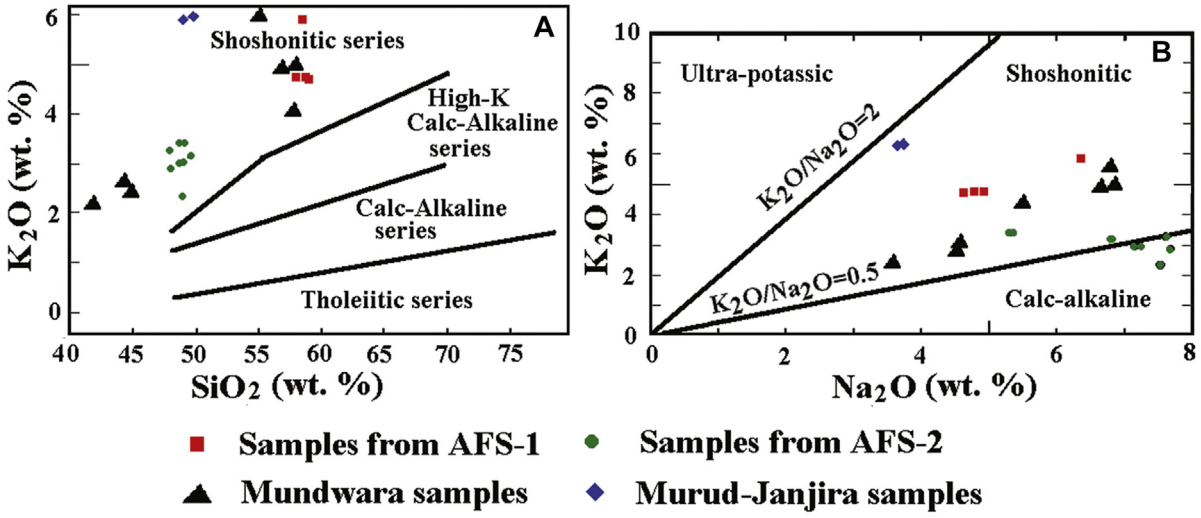


**Figure 9.** (A) $SiO_2$ (wt.%) vs. $K_2O$ (wt.%) plot (after Pearce et al., 1990) of the syenites from Deccan volcanic province. Note that all the samples fall in shoshonitic field. (B) $Na_2O$ (wt.%) vs. $K_2O$ (wt.%) plot (after Turner et al., 1996) of the syenites from Deccan volcanic province exhibiting shoshonitic affinity. Data for Mundwara is Subrahmanyam and Leelanandam (1989) and data for Murud-Janjira is from Dessai and Viegas (2010).

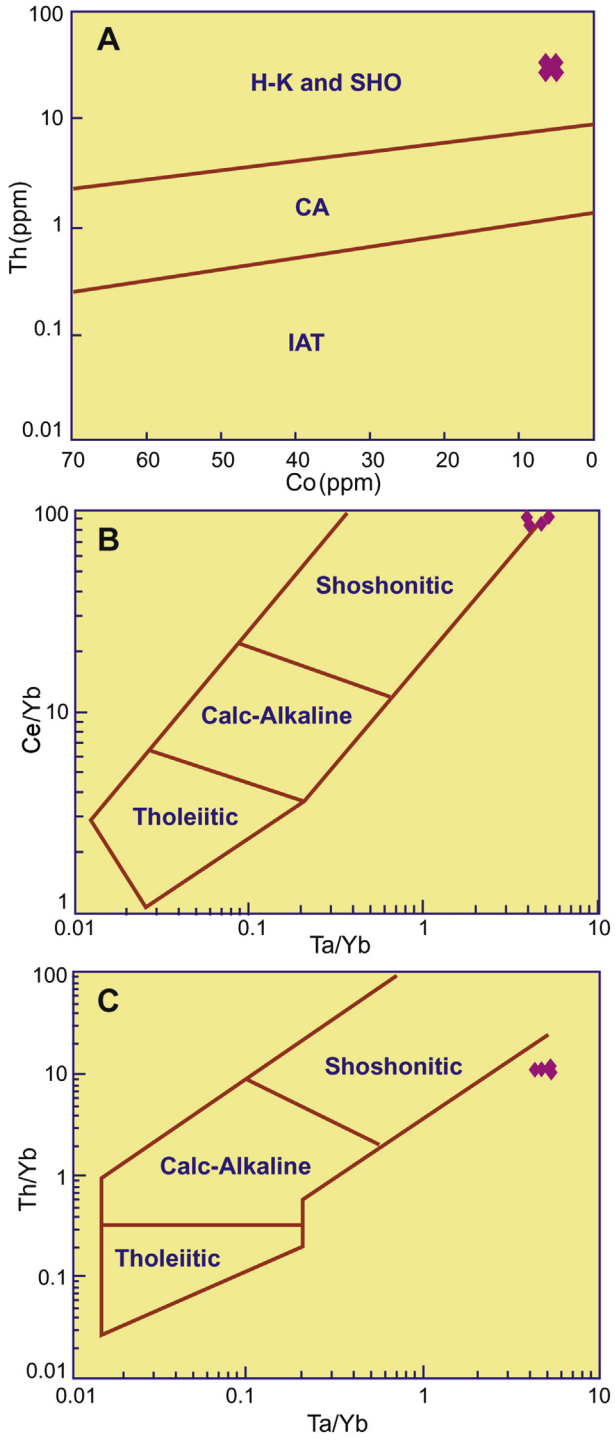


**Figure 10.** (A) Co (ppm) vs. Th (ppm) diagram with plots of AFS-1. The field demarcations are after Hastie et al. (2007). IAT– island arc tholeiite; CA – calc-alkaline; H-K and SHO – high-K calc-alkaline and shoshonite; (B) Ta/Yb vs. Ce/Yb plot (after Pearce, 1982) showing shoshonitic affinity of AFS-1; (C) Ta/Yb vs. Th/Yb plot (after Pearce, 1982) of AFS-1 exhibiting shoshonitic affinity.

and Becker, 1986; Macdonald and Scaillet, 2006; Brotzu et al., 2007) and (v) by magma mixing (Zhao et al., 1995; Stevenson et al., 1997; Vernikovsky et al., 2003; Jung et al., 2007; Ying et al., 2007).

Saha et al. (2011) while describing the occurrence of melanite garnet in syenite and ijolite-melteigite rocks of Mikir hills of Northeastern India pointed towards the role of fluid-enriched milieu in the magmatic history and effects of alkali metasomatism on the mineral paragenesis. Sreejith and Ravindra Kumar (2009) opined that the syenites from Kerala khondalite belt of South India signify crystallization of the rocks at shallow levels of the crust and the magma originated from enriched mantle. Subrahmanyam and Leelanandam (1989) favours liquid immiscibiliy as the main petrogenetic process for the formation of the Musala pluton of Mundwara igneous complex. Similar hypothesis has also been put forwarded by Mukhopadhyay et al. (2011) for the syenite and associated rocks of Elagiri complex of South Indian granulite terrain.

Hari (1998) and Chalapathi Rao et al. (2012) while discussing the petrogenesis of the lamprophyres from Chhotaudepur province concluded that these rocks are products of metasomatic mantle. Dessai and Viegas (2010) while describing the petrogenesis of alkaline rocks from Murud-Janjira, a part of Deccan volcanic province, inferred that the sodic and potassic lamprophyres are the most primitive among the rocks studied by them and may represent low degrees of melts of incompatible element-enriched mantle source. The samples of this study when plotted on Dy/Dy* vs. Dy/Yb (Fig. 12) fall towards the LREE enriched field. Further, the AFS-1 samples when plotted in the Ta/Yb vs. Th/Yb diagram (Fig. 13) clearly show its link with mantle metasomatism. Metasomatic process in the mantle redistributes incompatible elements and leads to an anomalous enrichments of these elements. Metasomatism is also evidenced by the enrichment of LREE and the presence of hydrous and other incompatible-element-rich phases. These phases are formed by the reaction of the metasomatic fluid (or melt) with anhydrous peridotite (Roden and Murthy, 1985). Conceição and Green (2004) opined that decompression melting of metasomatized lithospheric lherzolite with minor phlogopite and pargasite may produce primary shoshonitic magmas by dehydration melting at ~1 GPa, and 1050–1150 °C. The high incompatible elemental concentrations in AFS-2 samples support its metasomatic mantle origin. Orejana and Villaseca (2008) while discussing the heterogeneous metasomatism in cumulate xenoliths from Spanish Central System opined that carbonates, silicate and hydrous fluids or melts are the metasomatic agents and these agents could have been derived from the progressive differentiation of a $CO_2$-$H_2O$-rich highly alkaline magma.

Karmalkar and Rege (2002) while studying the alkaline rocks and the entrained mantle xenoliths in Kutch area, pointed out that the ratios of highly incompatible elements of both the alkaline rocks and the entrained mantle xenoliths are a consequence of melting of the metasomatized, subcontinental lithospheric mantle and the metasomatic activity can be attributed to the alkaline melts or fluid derived from the upwelling Reunion plume at the time of continental break-up. They further argued that the absence of typical 'metasomatic' minerals, low equilibration temperatures and enriched LREE patterns indicate that the upper mantle below Kutch underwent an event of cryptic metasomatic enrichment prior to partial melting. The distinctive chemical features, viz. LREE enrichment, strong Ti depletion relative to Eu, and slight Nb enrichment, fractionation of Zr and Hf are all results of interaction of refractory peridotite residues with carbonatite melts. The Ambadongar carbonatite ring complex lying very near to the present study area support the carbonate-rich metasomatism in this domain (cf:-Chalapathi Rao et al., 2012). The origin of metasomatized mantle rocks in the Deccan LIP can be correlated to the upwelling melts from the Réunion mantle plume (Chalapathi Rao and Lehmann, 2011; Chalapathi Rao et al., 2012). If we consider the views of Ju et al. (2013) that the initial and final phases of the Deccan volcanic eruptive activity were in the Narmada-Tapi and in the Western part of India, respectively, it can be concluded that the metasomatic fluids were active in the initial and final stages of the

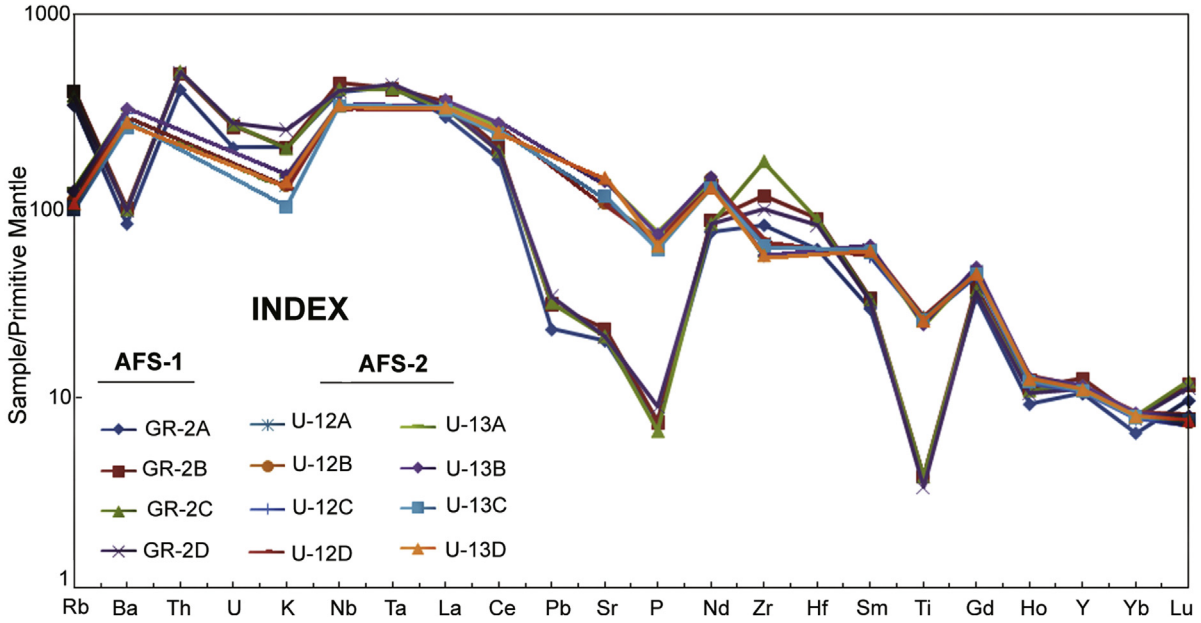


**Figure 11.** Primitive mantle normalized (after Sun and McDonough, 1989) multi-element spider diagram of alkali feldspar syenites from the Chhotaudepur province.

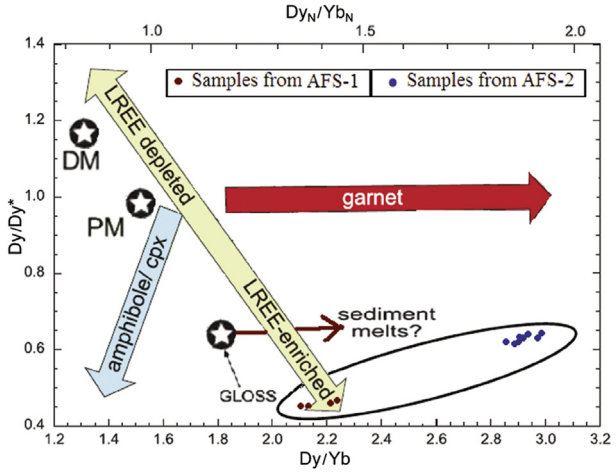


**Figure 12.** Dy/Dy* vs. Dy/Yb diagram (after Davidson et al., 2013) exhibiting LREE enrichment of the alkali feldspar syenites.

hot plume activity as lamprophyres, syenites and associated rocks in these regions are considered to be products of mantle metasomatism.

## 6. Conclusions

Two alkali feldspar syenite bodies from Phenai Mata igneous complex (AFS-1) and Karajwant (AFS-2) of Chhotaudepur sub-province exhibit different mineralogy and textures. Alkali feldspar syenite near Phenai Mata igneous complex (AFS-1) was reported by earlier workers as 'Pulaskite' whereas alkali feldspar syenite plug near Karajwant (AFS-2) is being reported for the first time. AFS-1 has hypidiomorphic texture and is characterized by the presence of feldspar ($Or_{55}Ab_{43}$ to $Or_{25}Ab_{71}$), ferro-pargasite/ferro-pargasite hornblende, hastingsite, pyroxene ($Wo_{47}$, $En_5$, $Fs_{46}$), magnetite and few biotite flakes. Hastingsite is seen as coronal rims around ferro-pargasite and also as discrete grains. AFS-2 exhibits a typical panidiomorphic texture with euhedral pyroxene ($Wo_{47-50}$, $En_{22-39}$,

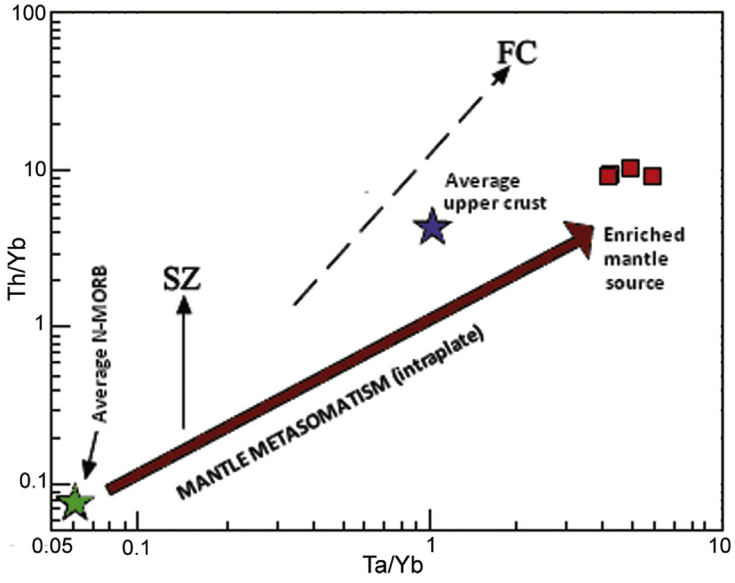


**Figure 13.** Alkali feldspar syenite (AFS-1) in terms of the Ta/Yb vs. Th/Yb diagram (after Pearce et al., 1990). SZ – Subduction zone; FC – fractional crystallization.

$Fs_{12-31}$) set in a groundmass matrix of alkali feldspar ($Or_{99}Ab_{0.77}$ to $Or_{1.33}Ab_{98}$), titanite and magnetite. AFS-2 exhibits higher elemental concentrations of Ba, Sr, and $\sum$REE. The average peralkaline index of the alkali feldspar syenites is around 1. Variation major and trace discrimination diagrams reveal that these alkali feldspar syenites have a shoshonite affinity and were derived from a within-plate and rifting environment. Negative Eu anomaly in the REE normalized diagram and the depletion of $K_2O$ and $Al_2O_3$ with MgO enrichment suggest feldspar fractionation. Crustal contamination, if any, is minimal and has little effect on the geochemistry. The enrichment of incompatible elements in alkali feldspar syenite of Chhotaudepur province suggests the role of mantle metasomatism. The origin of metasomatized mantle-derived rocks in the Deccan LIP can be correlated to the upwelling melts from the Réunion mantle plume.

## Acknowledgements

The financial support from Department of Science and Technology, New Delhi in the form of research grant (ESS/16/295/2006) to KRH and NVCR is acknowledged. Critical comments by two anonymous reviewers and editorial comments by H.M. Rajesh and M. Santosh are gratefully acknowledged.

## References

Basu, A.R., Renne, P.R., Das Gupta, D.K., Teichma, F., Poreda, R.J., 1993. Early and late alkali igneous pulses and a high $^3$He plume origin for the Deccan flood basalts. Science 261, 902–906.

Brotzu, P., Melluso, L., Bennio, L., Gomes, C.B., Lustrino, M., Morbidelli, L., Morra, V., Ruberti, E., Tassinari, C., D'Antonio, M., 2007. Petrogenesis of the Early Cenozoic potassic alkaline complex of Morro de São João, southeastern Brazil. Journal of South American Earth Sciences 24, 93–115.

Brown, P.E., Becker, S.M., 1986. Fractionation, hybridisation and magma-mixing in the Kialineq centre East Greenland. Contributions to Mineralogy and Petrology 92, 57–70.

Chakraborty, M.K., 1979. On the alkali syenites of mundwara suite, Sirohi district, Rajasthan. Proceedings of the Indian National Science Academy 45, 284–292.

Chalapathi Rao, N.V., Lehmann, B., 2011. Kimberlites, flood basalts and mantle plumes: new insights from the Deccan Large Igneous Province. Earth-Science Reviews 107, 315–324.

Chalapathi Rao, N.V., Burgess, R., Lehmann, B., Mainkar, D., Pande, S.K., Hari, K.R., Bodhankar, N., 2011a. $^{40}$Ar/$^{39}$Ar ages of mafic dykes from the Mesoproterozoic Chhattisgarh basin, Bastar craton, Central India: implication for the origin and spatial extent of the Deccan Large Igneous Province. Lithos 125, 994–1005.

Chalapathi Rao, N.V., Lehmann, B., Mainkar, D., Belyatsky, B., 2011b. Petrogenesis of the end-Cretaceous Behradih kimberlite (orangeite): implication for mantle plume-lithosphere interaction in the Bastar craton, Central India. Contributions to Mineralogy and Petrology 161, 721–742.

Chalapathi Rao, N.V., Dharma Rao, C.V., Das, Sanjay, 2012. Petrogenesis of lamprophyres from Chhota Udepur area, Narmada rift zone, and its relation to Deccan magmatism. Journal of Asian Earth Sciences 45, 24–39.

Chenet, A.L., Quidelleur, X., Fluteau, F., Courtillot, V., Bajpai, S., 2007. 40K–40Ar dating of the main Deccan large igneous province: further evidence of KTB age and short duration. Earth and Planetary Science Letters 263, 1–15.

Conceição, R.V., Green, D.H., 2004. Derivation of potassic (shoshonitic) magmas by decompression melting of phlogopite+pargasite lherzolite. Lithos 72, 209–229.

Currie, K.L., 1989. New ideas on an old problem: the peralkaline rocks. Geological Society of India Memoir 15, 117–136.

Davidson, J., Turner, S., Plank, T., 2013. Dy/Dy*: variation arising from mantle sources and petrogenetic processes. Journal of Petrology 54 (3), 525–537.

Deng, J., Yang, X., Sun, W., Huang, Y., Chi, Y., Yu, L., Zhang, Q., 2012. Petrology, geochemistry, and tectonic significance of Mesozoic shoshonitic volcanic rocks, Luzong volcanic basin, eastern China. International Geology Review 54 (6), 714–736.

DePaolo, D.J., 1981. Trace element and isotopic effects of combined wall rock assimilation and fractional crystallization. Earth and Planetary Science Letters 53, 189–202.

Dessai, A.G., Bodas, M.S., 1984. Occurrence of nepheline syenite around Murud-Janjira Raigarh district, Maharashtra, India. Current Science 53 (15), 775–777.

Dessai, A.G., Viegas, A., 2010. Petrogenesis of alkaline rocks from Murud-Janjira, in the Deccan Traps, Western India. Mineralogy and Petrology 98 (1–4), 297–311.

Dostal, J.B., Dupuy, C., 1984. Geochemistry of the North Mountain Basalts (Nova Scotia, Canada). Chemical Geology 45, 245–261.

Gwalani, L.G., Rock, N.M.S., Chang, W.J., Fernandez, S., Allegre, C.J., Prinzohofer, A., 1993. Alkaline rocks and carbonatites of Amba Dongar and adjacent areas, Deccan Igneous Province. Gujarat, India: geology, petrography and petrochemistry. Mineralogy and Petrology 47 (2–4), 219–253.

Gwalani, L.G., Fernandez, S., Karanth, R.V., Demeny, A., Chang, W.-J., Avasia, R.K., 1994. Alkaline and Tholeiitic Dyke Swarm associated with Amba Dongar and Phenai Mata complexes, Chhota Udaipur alkaline sub-province, Western India. Memoirs – Geological Society of India 33, 391–424.

Hari, K.R., 1998. Mineralogical and Petrological studies of the lamprophyres around Chhaktalao area, Madhya Pradesh. Journal Geological Society of India 51, 28–30.

Hari, K.R., Swarnkar, V., 2011. Petrogenesis of basaltic and doleritic dykes from Kawant, Chhotaudepur province, Deccan Traps. In: Srivastava, Rajesh (Ed.), Dyke Swarms: Keys for Geodynamic Interpretation. Springer-Verlag, Heidelberg, pp. 283–299.

Hari, K.R., Chalapathi Rao, N.V., Swarnkar, V., 2011. Petrogenesis of gabbro and orthopyroxene gabbro from the Phenai Mata Igneous Complex, Deccan volcanic province: a product of concurrent assimilation and fractional crystallization. Journal Geological Society of India 78, 501–509.

Hastie, A.R., Kerr, A.C., Pearce, J.A., Mitchell, S.F., 2007. Classification of altered volcanic island arc rocks using immobile trace elements: development of the Th-Co discrimination diagram. Journal of Petrology 48, 2341–2357.

Hofmann, C., Feraud, G., Courtillot, V., 2000. $^{40}$Ar/$^{39}$Ar dating of mineral separates and whole rocks from the Western Ghats lava pile: further constraints on duration and age of the Deccan Traps. Earth and Planetary Science Letters 180, 13–27.

Hooper, P.R., Widdowson, M., Kelley, S.P., 2010. Tectonic setting and timing of the final Deccan flood basalt eruptions. Geology 38 (9), 839–842.

Irvine, T.N., Baragar, W.R.A., 1971. A guide to the chemical classification of common volcanic rocks. Canadian Journal of Earth Sciences 8, 523–548.

Ju, W., Hou, G., Hari, K.R., 2013. Mechanics of mafic dyke swarms in the Deccan Large Igneous Province: palaeostress field modeling. Journal of Geodynamics 66, 79–91.

Jung, S., Hoffer, E., Hoernes, S., 2007. Neo-proterozoic rift-related syenites (Northern Damara Belt, Namibia): geochemical and Nd–Sr–Pb–O isotope constraints for mantle sources and petrogenesis. Lithos 96, 415–435.

Karkare, S.G., Srivastava, R.K., 1990. Regional dyke swarms related to the Deccan Trap Alkaline Province, India. In: Parker, A.J., Rickwood, P.C., Tucker, C.H. (Eds.), Mafic Dykes and Emplacement Mechanism. Balkema, Rotterdam, pp. 335–347.

Karmalkar, N.R., Rege, S., 2002. Cryptic metasomatism in the upper mantle beneath Kutch: evidence from spinel lherzolite xenoliths. Current Science 82 (9), 1157–1165.

Kumar, S., 1996. Geochemical specialization of Phenai Mata Igneous Complex, Baroda district, Gujarat. Journal of Scientific Research. 46, 207–218.

Kumar, S., 2003. Variation in the thickness of the lithosphere underneath the Deccan volcanic province, evidence from rare earth elements. Memoir Geological Society of India 52, 179–194.

Lan, T.G., Fan, H.R., Santosh, m., Hu, F.F., Yang, K.F., Yang, Y.H., Liu, Y., 2011. Geochemistry and Sr-Nd-Pb-Hf isotopes of the Mesozoic Dadian alkaline intrusive complex in the Sulu orogenic belt, eastern China: implications for crust-mantle interaction. Chemical Geology 285, 97–114.

Leake, B.E., 1978. Nomenclature of amphiboles. American Mineralogist 63, 1023–1052.

Leat, P.T., Thompson, R.N., Morrison, M.A., Hendry, G.L., 1998. Silicic magma derived by fractional-crystallization from Miocene minette, Elkhead Mountain, Colorado. Mineralogical Magazine 52, 577–585.

Lehmann, B., Burgess, R., Frei, D., Mainkar, D., Chalapathi Rao, N.V., Heaman, L.M., 2010. Diamondiferous kimberlites in Central India synchronous with the Deccan basalts. Earth and Planetary Science Letters 290, 142–149.

Li, Xianhua., Hanwen, Zhou., Chi-yu, Lee., Min, Sun., Chenhong, Chen, 2000. Shonshonitic intrusive suite in SE Guangxi: petrology and geochemistry. Chinese Science Bulletin 45, 653–659.

Litvinovsky, B.A., Jahn, B.M., Zanvilevich, A.N., Shadaev, M.G., 2002. Crystal fractionation in the petrogenesis of an alkali monzodiorite–syenite series: the Oshurkovo plutonic sheeted complex, Transbaikalia, Russia. Lithos 64, 97–130.

Macdonald, R., Scaillet, B., 2006. The central Kenya peralkaline province: insights into the evolution of peralkaline salic magmas. Lithos 91, 59–73.

Miyazaki, T., Kagami, H., Mohan, V.R., Shuto, K., Morikiyo, T., 2003. Enriched subcontinental lithospheric mantle in the northern part of the South Indian Granulite Terrain: evidence from Yelagiri and Sevattur syenite plutons, Tamil Nadu, South India. Gondwana Research 6, 585–594.

Morrison, G.W., 1980. Characteristics and tectonic setting of the shoshonite rock association. Lithos 13, 97–108.

Mukhopadhyay, S., Ray, J.S., Chattopadhyay, B., Sengupta, S., Ghosh, B., Mukhopadhyay, S., 2011. Significance of mineral chemistry of syenites and associated rocks of Elagiri Complex, Southern Granulite Terrane of the Indian Shield. Journal Geological Society of India 77, 113–129.

Müller, D., Rock, N.M.S., Groves, D.I., 1992. Geochemical discrimination between shoshonitic and potassic volcanic rocks in different tectonic settings: a pilot study. Mineralogy and Petrology 46, 259–289.

Nakamura, N., 1974. Determination of REE, Ba, Fe, Mg, Na and K in carbonaceous and ordinary chondrites. Geochimica et Cosmochimica Acta 38, 757–775.

Orejana, D., Villaseca, C., 2008. Heterogeneous metasomatism in cumulate xenoliths from the Spanish Central System: implications for percolative fractional crystallization of lamprophyric melts. In: Metasomatism in Oceanic and Continental Lithospheric Mantle. Geological Society, London. Special Publications 293, pp. 101–120.

Pearce, J.A., 1982. Trace element characteristics of lavas from destructive plate boundaries. In: Thorpe, R.S. (Ed.), Andesites: Orogenic Andesites and Related Rocks. John Wiley and Sons, Chichester, pp. 525–548.

Pearce, J.A., Bender, J.F., De Long, S.E., Kidd, W.S.F., Low, P.J., Güner, Y., Şaroğlu, F., Yilmaz, Y., Moorbath, S., Mitchell, J.G., 1990. Genesis of collision volcanism in Eastern Anatolia, Turkey. Journal of Volcanology and Geothermal Research 44, 189–229.

Rajesh, H.M., Chisonga, B.C., Shindo, K., Beukes, N.J., Armstrong, R.A., 2013. Petrographic, geochemical and SHRIMP U-Pb titanite age characterization of the Thabazimbi mafic sills: extended time frame and a unifying petrogenetic model for the Bushveld Large Igneous Province. Precambrian Research 230, 79–102.

Ray, J.S., Pande, K., Pattanayak, S.K., 2003. Evolution of the Amba Dongar Carbonatite Complex: constraints from $^{40}$Ar-$^{39}$Ar chronologies of the Inner Basalt and an alkaline plug. International Geology Review 45, 857–862.

Ray, R., Sheth, H.C., Mallik, 2007. Structure and emplacement of the Nandurbar-Dule mafic dyke swarm, Deccan Traps, and the tectonomagmatic evolution of flood basalts. Bulletin of Volcanology 69, 537–551.

Rios, D.C., Conceicao, H., Davis, D.W., Cid, J.P., Rosa, M.L.S., Macambira, M.J.B., McReath, I., Marinho, M.M., Davis, W.J., 2007. Paleoproterozoic Potassic-ultrapotassic Magmatism: Morro do Afonso Syenite Pluton. In: Precambrian Research, vol. 154. Elsevier, Bahia, Brazil, pp. 1–30.

Roden, M.F., Murthy, V.R., 1985. Mantle metasomatism. Annual Review of Earth and Planetary Science 13, 269–296.

Rogers, N.W., James, D., Kelley, S.P., De Mulder, M., 1998. The generation of potassic lavas from the eastern Virunga Province, Rwanda. Journal of Petrology 39, 1223–1247.

Saha, A., Ray, J.S., Ganguly, S., Chatterjee, N., 2011. Occurrence of melanite garnet in syenite and ijolite–melteigite rocks of Samchampi–Samteran alkaline complex, Mikir Hills, Northeastern India. Current Science 101 (1), 95–100.

Scarrow, J.H., Bea, F., Montero, P., Molina, J.F., 2009. Shoshonites, vaugnerites and potassic lamprophyres: similarities and differences between 'ultra' –high-K rocks. Earth and Environmental Science, Transactions of the Royal Society of Edinburgh 99, 159–175.

Simonetti, A., Bell, K., Viladkar, S.G., 1998. Isotopic data from the Amba Dongar carbonatite complex, West central India: evidence for an enriched mantle source. Chemical Geology 122, 185–198.

Sreejith, C., Ravindra Kumar, G.R., 2009. Petrological and geochemical characteristics of Marunthurkota syenites from the Kerala Khondalite Belt, southern India. Journal of the Geological Society of India 73, 386–392.

Stevenson, R., Upton, B.G.J., Steenfelt, A., 1997. Crust–mantle interaction in the evolution of the Ilímaussaq Complex, South Greenland: Nd isotopic studies. Lithos 40, 189–202.

Streckeisen, A.L., 1974. Classification and nomenclature of plutonic rocks. Geologische Rundschau 63 (2), 773–786.

Subrahmanyam, N.P., Leelanandam, C., 1989. Differentiation due to probable initial immiscibility in the Musala pluton of the Mundwara alkali igneous complex, Rajasthan, India. Memoirs Geological Society of India 15, 25–46.

Sukeshwala, R.N., Avasia, R.K., 1972. Carbonatite – alkalic complex of Panwad – Kawant, Gujarat and its bearing on the structural characteristics of the area. Bullettin of Volcanology 35, 564–578.

Sukheswala, R.N., Sethna, S.F., 1973. Oversaturated and undersaturated differentiates in the tholeiitic igneous complex of Phenai Mata, Baroda District, Gujarat State. Neues Jahrbuch für Mineralogie 118, 159–176.

Sun, S.-s., McDonough, W.F., 1989. Chemical and Isotopic Systematics of Oceanic Basalts: Implications for Mantle Composition and Processes, vol. 42. Geological Society Special Publication, pp. 313–345.

Taylor, S.R., McLennan, S., 1995. The geochemical composition of the continental crust. Reviews of Geophysics 33, 241–265.

Thompson, R.N., Dickin, A.P., Gibson, I.L., Marrison, M.A., 1982. Elemental fingerprints of isotopic contamination of Hebridean Paleocene mantle-derived magmas by Archean sial. Contributions to Mineralogy and Petrology 79, 159–168.

Thompson, R.N., Morrison, M.A., Hendry, G.L., Parry, S.J., 1984. An assessment of the relative roles of a crust and mantle in magma genesis: an elemental approach. Royal Society of London Philosophical Transactions A310, 549–590.

Turner, S., Arnaud, N., Liu, J., Rogers, N., Hawkesworth, C., Harris, N., Kelley, S., Calsteren, P.V., Deng, W., 1996. Post-collision, Shoshonitic volcanism on the Tibetan Plateau: implications for convective thinning of the lithosphere and the source of ocean island basalts. Journal of Petrology 37 (1), 45–71.

Vanderkluysen, L., Mahoney, J.J., Hooper, P., Sheth, H., Ray, R., 2011. The feeder system of the Deccan Traps (India): insights from dike geochemistry. Journal of Petrology 52, 315–343.

Vernikovsky, V.A., Pease, V.L., Vernikovskaya, A.E., Romanov, A.P., Gee, D.G., Travin, A.V., 2003. First report of early Triassic A-type granite and syenite intrusions from Taimyr: product of the northern Eurasian superplume? Lithos 66, 23–36.

Viladkar, S.G., 1984. Alkaline Rocks Associated with the Carbonatites of Amba Dongar, Chhota Udaipur, Gujarat, India. Sukheswala. Indian Mineralogist 130–135.

Viladkar, S.G., Avasia, R.K., 1992. Pyroxenes from alkaline rocks of the Chhota Udaipur carbonatite-alkaline province, Gujarat, India. Journal of the Geological Society of India 39, 313–319.

Wang, Q., Li, J.W., Jian, P., Zhao, Z.H., Xiong, X.L., Bao, Z.W., Xu, J.F., Li, C.F., Ma, J.L., 2005. Alkaline syenites in eastern Cathaysia (South China): link to Permian–-Triassic transtension. Earth and Planetary Science Letters 230, 339–354.

West Jr., D.P., Tomascak, P.B., Coish, R.A., Yates, M.G., Reilly, M.J., 2007. Petrogenesis of the ultrapotassic Lincoln syenite, Maine: late Silurian. American Journal of Science 307, 265–310.

Widdowson, M., Pringle, M., Fernandez, O.P., 2000. A post K–T boundary (Early Palaeocene) age for Deccan-type feeder dykes, Goa, India. Journal of Petrology 41, 1177–1194.

Wyborn, D., 1992. The tectonic significance 496 of Ordovician magmatism in the eastern Lachlan Fold Belt. Tectonophysics 214, 177–192.

Ying, J.F., Zhang, H.F., Sun, M., Tang, Y.J., Zhou, X.H., Liu, X.M., 2007. Petrology and geochemistry of Zijinshan alkaline intrusive complex in Shanxi Province, western North China Craton: implication for magma mixing of different sources in an extensional regime. Lithos 98, 45–66.

Zhang, Z., Xiao, X., Wang, J., Wang, Y., Kusky, T.M., 2008. Post-collisional Plio-Pleistocene shoshonitic volcanism in the western Kunlun Mountains, NW China: geochemical constraints on mantle source characteristics and petrogenesis. Journal of Asian Earth Sciences 31, 379–403.

Zhao, J.-X., Shiraishi, K., Ellis, D.J., Sheraton, J.W., 1995. Geochemical and isotopic studies of syenites from the Yamoto Mountains East Antartica: implication for the origin of syenitic magmas. Geochimica et Cosmochimica Acta 59, 1363–1385.